




# Interaction of the Sea Breeze with the Urban Area of Rome: WRF Mesoscale and WRF Large-Eddy Simulations Compared to Ground-Based Observations

Annalisa Di Bernardino<sup>1</sup>  · Vincenzo Mazzeola<sup>2,3</sup> · Mattia Pecci<sup>4,5</sup> · Giampietro Casasanta<sup>6</sup> · Marco Cacciani<sup>1</sup> · Rossella Ferretti<sup>2</sup>

Received: 8 September 2021 / Accepted: 19 July 2022 / Published online: 10 August 2022  
© The Author(s) 2022

## Abstract

The Weather Research and Forecast (WRF) model is used to simulate atmospheric circulation during the summer season in a coastal region of central Italy, including the city of Rome. The time series of surface air temperature, wind speed, and direction are compared with in situ observations in urban Rome and its rural surroundings. Moreover, the vertical wind profiles are compared to sodar urban measurements. To improve the WRF model's ability to reproduce the local circulation, and the onset and propagation of the sea breeze, several simulations are carried out modifying the land use and the thermal and physical properties of the surfaces. Based on the results of the correlation coefficient and the RMSE, the heat capacity and albedo are the parameters mostly influencing the daily temperature cycle. Particularly, the temperature in the urban area is reproduced more realistically when the heat capacity is increased. Hence, the best simulations are used to initialize a large-eddy simulation at high spatial resolution to analyze the interaction between the sea breeze and the urban heat island and to investigate the interaction of the sea breeze front with orography and surface roughness. As confirmed by observations collected by in situ weather stations in the surroundings of Rome, the front, entering the city, splits into three branches: (i) a west component in the

---

Marco Cacciani: Deceased January 18, 2022.

---

✉ Annalisa Di Bernardino  
annalisa.dibernardino@uniroma1.it

<sup>1</sup> Department of Physics, Sapienza University of Rome, 00185 Rome, Italy

<sup>2</sup> CIMA Research Foundation, 17100 Savona, Italy

<sup>3</sup> Department of Physical and Chemical Sciences, Centre of Excellence CETEMPS, University of L'Aquila, 67100 L'Aquila, Italy

<sup>4</sup> Department of Information Engineering, Electronics and Telecommunications (DIET), Sapienza University of Rome, 00185 Rome, Italy

<sup>5</sup> Laboratory for Observations and Analyses of Earth and Climate, National Agency for New Technologies, Energy, and Sustainable Economic Development (ENEA), 00123 Rome, Italy

<sup>6</sup> National Research Council of Italy, Institute of Atmospheric Sciences and Climate (CNR-ISAC), 00133 Rome, Italy

western flank of the city, closer to the sea; (ii) a north-west component in the northern, inland side, and (iii) a south-west component in the south area of the city.

**Keywords** Ground-based measurements · Large-eddy simulation · Local circulation · Sea breeze · Weather Research and Forecasting

## 1 Introduction

Land use and land cover have a remarkable impact on local-scale meteorology, affecting rainfall (Pielke et al. 2007; Satya et al. 2020) and air quality (Wu et al. 2012), with impacts on human comfort and health (Lo and Quattrochi 2003).

In metropolitan areas, where most of world population lives (UN 2018) and where the most evident manifestation of the impact of anthropization on the climate is the urban heat island (UHI) phenomenon, this is a relevant problem. The UHI phenomenon is a well-known problem leading to higher temperatures in urbanized areas (Oke 1973), clearly appearing during night-time and with low wind speed. Although the effects of UHIs at the surface are clear during the night, the vertical structure of the planetary boundary layer (PBL) is deeply affected by UHIs during the day. Urban heat islands develop in both large and small cities, no matter if they are located in a warm or cold climate (Stewart and Oke 2012), mainly because of the higher release of anthropogenic heat due to transportation, industries, and domestic heating, among others. Moreover, a decrease in the surface evapotranspiration is caused by asphalt and concrete, and the high density of buildings with complex geometry modifies the airflow close to the ground, reducing ventilation, cooling, and leading to stagnation phenomena. Nevertheless, as shown in this work, the wind field can also largely influence the UHI intensity and, if calm wind conditions occur, the shadow effect of the urban buildings can reduce their daytime temperatures, slowing down the heat energy accumulation and its release into the atmosphere (Zhang et al. 2017; Lian et al. 2018), resulting in lower temperatures in the urban area than in the rural surroundings. Furthermore, UHIs may exacerbate local air pollution, reduce visibility (Witiw et al. 2003), influence agriculture by requiring increased water usage (Kumar et al. 2017), and increase human discomfort because of more intense and longer heat waves in cities (Tan et al. 2010). Recently, considerable advances have been made in understanding and modelling the effects of UHIs thanks to numerical simulations (O'Malley et al. 2015; Sun et al. 2020; Litardo et al. 2020), also aimed at defining efficient mitigation strategies (Solecki et al. 2005; Wang et al. 2016). One of the most widely used numerical models is the Weather Research and Forecasting (WRF) model, which is able to reproduce the urban canopy effect on urban area circulation, allowing the user to choose from different urban parametrizations. In 2011, Chen et al. (2011) reviewed the different urban canopy schemes available in WRF, including the bulk urban parametrizations (Liu et al. 2006), the single-layer Urban Canopy Model (UCM) (Kusaka et al. 2012), and the Building Environment Parameterization (BEP) model (Martilli et al. 2002). Several studies demonstrated that high-resolution mesoscale simulations need a careful choice of urban parameters to accurately reproduce the UHI effect, and yet that several unsolved problems must be considered, such as the inadequate description of land cover data (Oke 1988). Chen et al. (2014) used WRF to represent different urbanization scenarios for Hangzhou City, China, with a detailed urban land map. An ideal simulation with the entire urban surface replaced with cropland was also carried out. The results showed that the simulated UHI effects were primarily due to the urban land use and to the release of anthropogenic heat. Nevertheless, the simulation

of the UHI often is not detailed enough for both metropolises and small towns. For instance, Jin et al. (2005) investigated the effect of surface temperature, albedo, and emissivity on UHI considering different urban settings (e.g. New York, Phoenix, and Beijing) and comparing numerical results with satellite-measured skin temperatures. They found a deeper UHI effect at both daytime and night-time, rather than at night, as suggested from surface air temperature measurements, using the skin temperature. Gohil and Jin (2019) modelled the UHI in the small city of College Park (Maryland, USA) using the BEP scheme for various seasons and clear and cloudy days. They compared the simulated and observed 2-m-temperature trend showing systematic errors at night, with overestimations and underestimations up to 5 °C both in urban and rural areas. They also stressed the parametrization of temperature, solar radiation, and soil moisture to improve the agreement between numerical simulations and measurements.

In the last few years, the urban area of Rome has been studied using WRF with different goals. To the aim of simulating the circulation in the city, Pichelli et al. (2014) performed a sensitivity study. The numerical results for wind, air temperature, turbulent fluxes, PBL height, and water vapour mixing ratio, obtained using different PBL parametrizations, were compared with satellite and urban ground-based observations. Moreover, they reproduced the circulation in a statistically relevant episode using different PBL schemes and UCMs. Their findings show a general overestimation of the vertical transport of horizontal momentum from upper levels to the low atmosphere when mesoscale forcing prevails. Morini et al. (2018) demonstrated that an accurate parametrization of the urban morphology for the city of Rome can lead to a more accurate simulation of the UHI using WRF. Their results showed that increased albedo could favour the UHI mitigation, reducing the temperature in the urban area up to 4 °C during daytime. Ciancio et al. (2018) used WRF to set a climate database for the investigation of the annual energy consumption of a building located in the city centre of Rome. They proved that, by neglecting the effect of the UHI, the estimated energy consumption due to the building cooling was underestimated by 35–50%. Finally, Keppas et al. (2021) use WRF weather simulation to investigate the climate change impact on UHI for both Rome and Thessaloniki. They found a UHI intensity of approximately 1.5–3 °C at night and in the early morning (time interval 2006–2010), whereas no large variations were found considering future climate change in the time intervals 2046–2050 and 2096–2100.

Generally, mesoscale numerical models are not able to capture the microscale dynamics, therefore, to further investigate the processes at the small-scale variability a higher spatial resolution is needed. In the last few years, the increased availability of computer power, allowed for the use of more accurate models and large-eddy simulations (LES). The LESs explicitly resolve energy-containing turbulent motions and are used for a large variety of applications, such as urban impact on microclimate, transport of pollutants, and convective processes within the PBL (Moeng et al. 1996; Siebesma et al. 2003; Bryan et al. 2008). Moreover, LES allows for the investigation of PBL regimes, interaction of atmospheric flow over complex orography, and abrupt change in land cover (Bou-Zeid et al. 2004; Courault et al. 2007; Chan 2009; Rotunno et al. 2009; Stoll and Porté-Agel 2009). Here, LESs are used to further investigate the effect of UHI in Rome.

The aim of this paper is the in-depth investigation of the circulation in the central region of Italy, including the city of Rome, by numerical modelling and ground-based observations. A few preliminary simulations are performed using WRF to better represent the urban area of Rome, by varying the land cover dataset and the thermal and physical urban parameters. Then, heat capacity, thermal conductivity, albedo, and emissivity of roofs, buildings, and ground are changed to investigate their role in the local circulation and to test the sensitivity of WRF to these variables. Moreover, the urban geometry, in terms of percentage of buildings with a

given height, street direction, and related buildings height and width, is modified. The results are compared with the vertical profiles of wind speed and direction measured in downtown Rome, as well as with air temperature, wind speed, and direction collected by ground-based meteorological stations located both in Rome and in its surroundings. Then, the correlation coefficient is used to identify the most realistic simulation. Finally, the best WRF outputs are used to initialize two LES simulations at high-spatial-resolution circulation in the urban domain to highlight the role of the UHI and its interaction with the sea breeze front.

The paper is structured as follows: Sect. 2 presents the case study, the in situ measurements, and the set-up of the sensitivity experiments. In Sect. 3, the main results are presented and discussed, while the conclusions are drawn in Sect. 4.

## 2 Material and Methods

### 2.1 Case Study

To the aim of investigating the local circulation in the urban area of Rome, the meteorological conditions that occurred during 28–30 June 2011 are considered. The selected days are part of the intensive field campaign URBan Sustainability Related to Observed and Monitored Aerosol (URBS-ROMA) that took place from 20 June to 20 July 2011, aimed to characterize the atmospheric aerosol properties in the urban environment during the summer (Campanelli et al. 2019).

On 28–30 June 2011, the synoptic scenario was characterized by upper-level high pressure over the central Mediterranean constrained by a deep low intrusion from Iceland located on the north side of the Alps, and a cyclonic system over the Balkans region. On 28 June, a surface high pressure with smoothed gradients ensured stable atmospheric conditions with north-westerly advection over the western Mediterranean area. During 29 June 2011, the upper-level high pressure started to move eastward, slightly increasing the surface gradients (see Fig. 1). By 30 June 2011, a tongue of deep low pressure from Iceland moved south-eastward approaching northern Italy producing a south-westerly flow, which brought warmer and more humid air. The advection of warm and humid air at low levels, associated with cold air at upper levels, reduced the stability of the atmosphere, causing precipitation along the mountainside and an increase in cloud cover over most of the Italian peninsula.

These two days were selected because of the smooth pressure gradients over Italy, which allowed the local circulation to develop. Indeed, 28 June 2011 was characterized by a clear sea breeze circulation, as recorded by most of the surface stations in the rural area near Rome (Fig. 10), whereas the day after the large-scale and the local forcings started to interact, reducing the strength of the sea breeze circulation. This meteorological structure allows for analysing the intrusion of the sea breeze front inland, the interaction with the UHI, and the WRF ability to correctly reproduce the local forcing (see Sect. 3.3 for details about the simulation of the inland propagation of the sea breeze regime).

### 2.2 Observations

A sodar system has been operating since 2007 (Iannarelli et al. 2021) on the rooftop of the Physics Department of the University of Rome “La Sapienza”, a six-story building where the Atmospheric Physics Laboratory (hereinafter, APL, Lat. 41.90° N, Long. 12.51° E, 75 m above sea level, a.s.l.) hosts the urban location of the Boundary-layer Air Quality-analysis

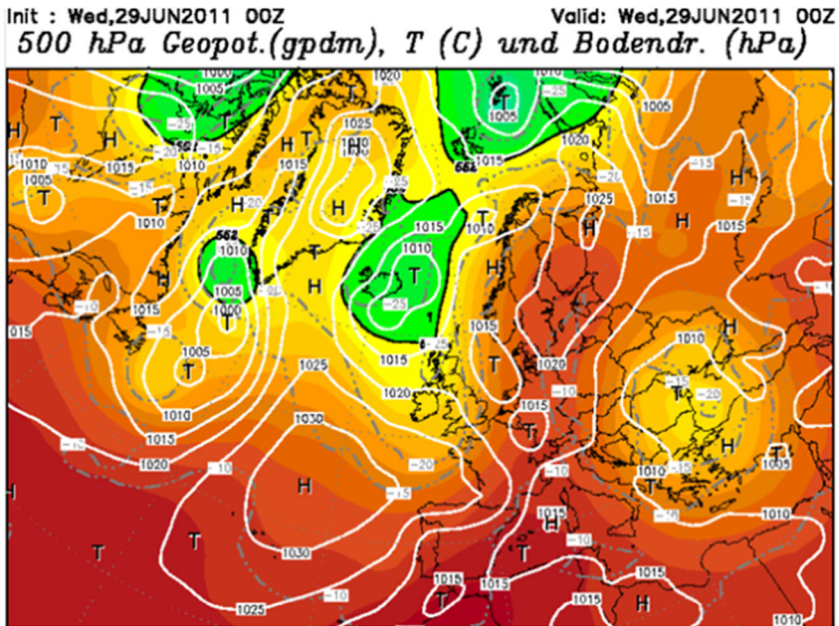


**Fig. 1** Synoptic weather conditions on 29 June 2011 at 0000 UTC. Geopotential at 500 hPa (colours), surface pressure (hPa, white lines), and temperature ( $^{\circ}\text{C}$ , dashed grey lines). *Source:* <https://www.wetterzentrale.de/>

Using Network of Instruments (BAQUNIN, <https://www.baqunin.eu/>) atmospheric super-site (Iannarelli et al. 2021). The building is about 25-m high and is located on a highly urbanized and heterogeneous area downtown. The sodar operates routinely in a three-axial, monostatic configuration, with a pulse repetition period of 6 s. Two antennae are tilted  $20^{\circ}$  from the Zenith, pointing north and east, while the third antenna is positioned vertically. The three antennae simultaneously emit 100-ms-long acoustic bursts, centred at 1750, 2000, and 2250 Hz, respectively, allowing for a maximum probing range of 1000 m with a vertical resolution of 28.4 m. The retrieved signal allows for obtaining instantaneous vertical profiles of radial velocities and 10-min-averaged profiles of wind speed and direction. Details on the retrieval procedure can be found in Mastrantonio and Fiocco (1982), Mastrantonio et al. (1994), and Casasanta et al. (2014). As the measurements are carried out in an urban environment, noisy vertical wind velocity profiles and spikes are discarded.

Moreover, hourly wind velocity and direction, and hourly air temperature at 2 m a.g.l. are obtained from ground-based meteorological stations, belonging to the Regional Agency for the Development and Innovation of Agriculture of Lazio (ARSIAL, <http://www.arsial.it/arsial/>). The network consists of a large number of sites, distributed throughout the region. In this work, only a few stations are selected to evaluate the role of the UHI in the local circulation, also located nearby Rome. All the ARSIAL weather stations considered here have been active since 2004, except for RM-L, which has been operational since 2005. Table 1 provides geographical information about the in situ stations used in this study, whereas their location, together with APL, is shown in Fig. 2b.

The stations of Montelibretti (hereinafter, ML), Palombara (PA), Marcellina (MA), Roma–Ponte di Nona (RM-P), Marino (MN), and Roma–Capocotta (RM-C) are equipped with CR1000 Campbell instruments (Campbell Scientific Europe, Loughborough, U.K.). The

**Table 1** Outline of ARSIAL in situ meteorological stations considered

Station	Station ID	Latitude	Longitude	Altitude (m a.s.l.)				
Roma—Via Lanciani	RM-L	41.92° N	12.52° E	26				
Montelibretti	ML	42.15° N	12.72° E	148				
Monterotondo	MR	42.08° N	12.65° E	100				
Palombara	PA	42.07° N	12.74° E	140				
Marcellina	MA	42.00° N	12.80° E	164				
Roma-Ponte di Nona	RM-P	41.90° N	12.65° E	62				
Zagarolo	ZA	41.85° N	12.80° E	255				
Monteporzio	MP	41.80° N	12.71° E	583				
Marino	MN	41.75° N	12.63° E </tr <tr> <td>Roma—Capocotta</td> <td>RM-C</td> <td>41.69° N</td> <td>12.45° E</td> <td>90</td> </tr>	Roma—Capocotta	RM-C	41.69° N	12.45° E	90
Roma—Capocotta	RM-C	41.69° N	12.45° E	90				

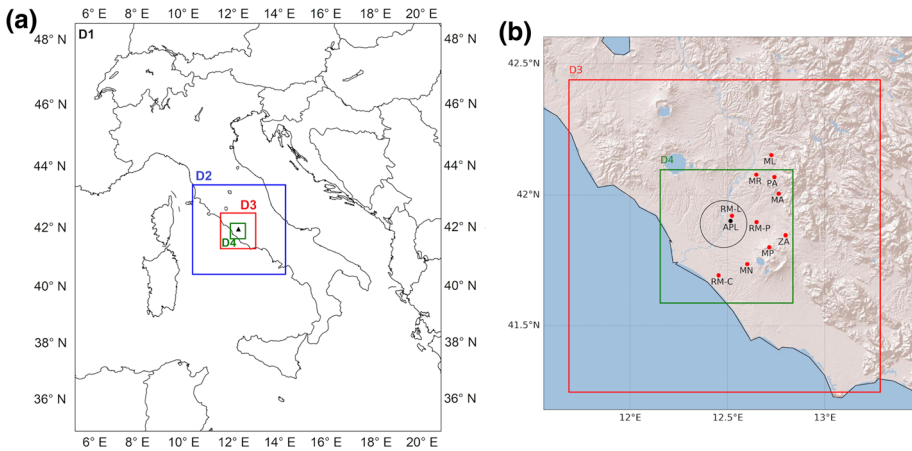


**Fig. 2** **a** WRF domains configuration used for the present study: the national (D1, black box) and the regional (D2, blue box) domains are used for the default investigations; D3 and D4 (red and green boxes, respectively) are added for the LES(s) (see Sect. 3.4). The black triangle indicates the location of Rome. **b** Zoom of D3 and D4 with the geographical distribution of the ARSIAL stations (red dots) and the APL site (black dot). The black circle indicates, approximately, the limit of the urban area of Rome

sensors of Monterotondo (MR) and Monteporzio (MP) stations are Siap + Micros DA9000 (San Fior, Treviso, Italy), while Zagarolo (ZA) and Roma–Via Lanciani (RM-L) stations are equipped with CR10X Campbell (Campbell Scientific Europe, Loughborough, U.K.) and CR510 Campbell (Campbell Scientific Europe, Loughborough, U.K.) sensors, respectively. All the stations are positioned at the ground, except for RM-L, which is installed on the roof of a 5-storey building. All sensors comply with WMO (World Meteorological Organization) requirements, except for their positioning, since the anemometers are installed at 2 m above the ground. Datasets are provided with hourly resolution and are pre-processed and validated by ARSIAL, although no exact information about data uncertainty is currently available.

## 2.3 Model set-up and scenarios

The Advanced Research WRF (ARW) model (Skamarock et al. 2019), version 4.0.0, used for the numerical simulations, is a fully compressible, non-hydrostatic model, with terrain-following coordinates and Arakawa C staggering grid, developed by the National Center for Atmospheric Research (NCAR) laboratories in collaboration with other research institutes.

The model set-up is the following. A two-way nesting is used for this study: the father domain (D1) covers entire Italy with a spatial resolution of 3 km, and the nested one (D2) covers central Italy with a 1 km grid spacing (Fig. 2, black and blue boxes, respectively). Domains 3 and 4 (Fig. 2, red and green boxes, respectively) with a spatial resolution of 333 m and 111 m, respectively, are used for the LES(s) presented in Sect. 3.4. A total of 40 hybrid unequally spaced vertical levels are considered from the ground level up to 100 hPa, with the first level of the model at about 14 m, i.e. below the average height of the buildings in the centre of Rome.

Based on the operational configuration of the meteorological-hydro chain at the CETEMPS Center of Excellence of the University of L'Aquila (Ferretti et al. 2020), the following physical parameterizations are chosen. The long- and shortwave radiation are parameterized using Dudhia (Dudhia 1989) and the Rapid Radiative Transfer Model (RRTM) schemes (Mlawer et al. 1997), respectively. For cloud microphysics, the WSM6 scheme (Hong and Lim 2006) with six different types of hydrometeors is applied. The Noah Land Surface Model is used for the land surface processes. Finally, the physical processes in the PBL are parameterized in D1 and D2 using the Mellor–Yamada–Janjić scheme (Janjić 1994). In addition, the default 21 MODIS land use categories (30 s in resolution, Friedl et al. 2001) derived from MODIS are used.

Lastly, the BEP parameterization (Martilli et al. 2002) is applied for the urban surface, where a multi-layer urban canopy model is defined. In this scheme, the three-dimensional structure of an urban area is accounted for by recognizing three different urban surfaces in the urban canopy layer: roofs, roads, and vertical walls. Sources and sinks of heat, moisture, and momentum due to the presence of buildings are also considered. Finally, BEP interacts with the PBL allowing for the highest buildings to exceed the lowest model levels and is conceived to have vertical levels located within the urban canopy. The choice of a BEP scheme was based on previous studies showing better results in urban areas (e.g. Salamanca et al. 2018). Moreover, if BEP is associated with the Building Energy Model (BEM), the anthropogenic heat is also estimated (Salamanca et al. 2011), but it is not used in this study. As a future step, we plan to use the best configuration found in this paper to evaluate the improvement of using the BEM parametrization.

For all the experiments, except for the LES, the European Centre for Medium-Range Weather Forecasts (ECMWF) Integrated Forecasting System (IFS) operational forecast provided the initial and boundary conditions with horizontal resolution of 0.1°. For the LES experiment, as discussed in Sect. 3.4, the output of the best WRF configuration is used to initialize the model.

The rationale of the experiments performed in this study is the following: (1) a control simulation is carried out and used as reference; (2) the land use is improved by implementing the Coordinated Information on the European Environment (CORINE) dataset and the geometry of the buildings is defined to correctly represent the local forcing; (3) a set of tuning experiments are performed to improve the model ability to reproduce the thermal and physical characteristics of the urban area of Rome; (4) the best WRF configuration is used to force a LES to investigate the circulation of downtown Rome.

The control run (WRF\_CNTR) is a preliminary simulation using the default values (Ferretti et al. 2020) together with the MODIS land use. Then, the WRF\_CORINE simulation is performed by using the more accurate and recent land use data from the 2018 CORINE dataset (EEA 2018). In this configuration, the 44 classes are remapped in 24 categories (see Fig. 3) following Pineda et al. (2004). The differences between CORINE and MODIS are clearly shown in the urban area, where green spots are represented by CORINE only (Fig. 3). Moreover, the large urban area south of Rome, present in MODIS, is largely reduced by CORINE, in agreement with the actual definition of rural and urban areas in the neighbourhood of Rome. This simulation also allows for investigating the role of the land use in both the sea-breeze regime evolution entering inland and the development of the UHI.

Moreover, a tuning of the BEP parameters for the city of Rome is performed by defining the geometry of the buildings, expressed as a percentage of the buildings with a given height and width, together with the direction and length of the streets (Table 2). As a first approximation, streets and buildings are considered as oriented along the north–south and east–west directions, which is not a too strong approximation for Rome, i.e. a city with a complex structure where large part was built during the Umbertine period following a well-defined

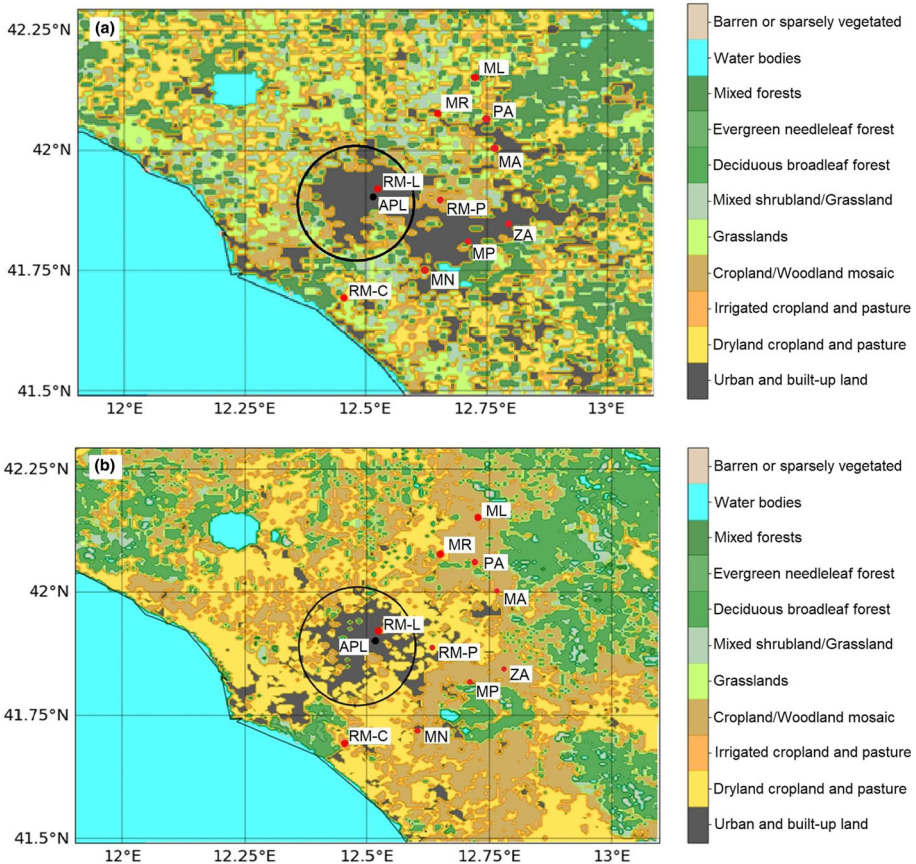


**Fig. 3** Land cover maps obtained using **a** MODIS and **b** CORINE datasets. Note that the different classification of the two datasets has been standardised to facilitate the data comparison



**Table 2** Building heights and the relative percentage considered in the present study

Building height (m)	% of Buildings
10	10
15	30
18.5	60

geometric architecture. According to Morini et al. (2018), the mean street width and the width of the mean buildings are set to 20 m and 19 m for the north–south direction and to 19 m and 22 m for the east–west direction, respectively.

Furthermore, to take into account the heterogeneity of the urban area of Rome, characterized by a packed urban centre and scattered suburbs, WRF simulations were performed by differentiating urban land use in the three subclasses provided by BEP, i.e. high density, low density, and commercial. Despite this more detailed classification, no significant improvements are found, and, for this reason, the authors choose to carry out all the simulations presented hereinafter considering a single urban class.

The comparison of the time series for wind speed, wind direction, and air temperature near the surface, between WRF\_CORINE and WRF\_CNTR, presented in Sect. 3.2.1, clearly shows that CORINE dataset improve the results by reproducing more accurately the atmospheric variables.

A set of simulations are carried out to tune the BEP scheme to the thermal and physical characteristics of Rome by using the WRF\_CORINE configuration and the chosen geometrical parameters. The following thermal parameters are varied:

- (i) The heat capacity of roofs (*CAPR*), buildings (*CAPB*), and ground (*CAPG*);
- (ii) The thermal conductivity of roofs (*AKSR*), buildings (*AKSB*), and ground (*AKSG*);
- (iii) The albedo of roofs (*ALBR*), buildings (*ALBB*), and ground (*ALBG*);
- (iv) The emissivity of roofs (*EPSR*), buildings (*EPSB*), and ground (*EPSG*).

These parameters have been changed, one by one, with the twofold purpose of investigating their role both in the urban area circulation and in the development of the UHI. Hence, the following experiments have been performed:

1. WRF\_CAP, the default values of thermal capacities (*CAPR*, *CSPB*, and *CAPG*) have been changed to  $2.1 \times 10^6 \text{ J m}^{-3} \text{ K}^{-1}$ , based on Falasca and Curci (2018). They evaluated the thermal capacities for the city of Milano (Italy), i.e. a town with dimension and population density comparable to Rome.
2. WRF\_COND, the thermal conductivity of roofs (*AKSR*), buildings (*AKSB*), and ground (*AKSG*) have been tuned. The parameters are modified according to Falasca and Curci (2018) and the default values are changed into  $2.28 \text{ J s}^{-1} \text{ K}^{-1}$  for *AKSR* and *AKSB*, and  $0.7 \text{ J s}^{-1} \text{ K}^{-1}$  for *AKSG*, respectively. This experiment allows for improving the model temperature diurnal variation in the metropolitan area.
3. WRF\_ALB, the albedo in the urban area is tuned. The values of albedo for roofs, buildings, and the ground are decreased to 0.12, being this value the average albedo of asphalt concrete (Sugawara and Takamura 2014). This experiment also allows for investigating the sensitivity of WRF to the albedo in reproducing the local circulation.
4. WRF\_EMS, the emissivity in the urban area is tuned. Based on Falasca and Curci (2018) the values of *EPSR*, *EPSB*, and *EPSG* are increased from 0.90 to 0.97, to further improve the reproduction of the diurnal variation of air temperature.

5. WRF\_ALL, all the modifications to the physical and thermal parameters carried out individually in the previous simulations are implemented, to evaluate the overall effect.

A few more simulations are carried out to investigate the sensitivity of WRF to both albedo and heat capacity, by varying individually the two parameters starting from WRF\_ALL. In the first two simulations the surfaces albedo are modified: following Morini et al. (2018)  $ALBR = 0.65$ ,  $ALBB = 0.60$ ,  $ALBG = 0.45$  have been set in WRF\_ALB1, whereas a value of 0.28 has been set for  $ALBR$ ,  $ALBB$ , and  $ALBG$  in WRF\_ALB2. Similarly, two more experiments are performed to explore the role of these parameters in driving the model temperature. Therefore, the heat capacity only is modified by setting the CAPs values to large and not realistic values:  $5.0 \times 10^6 \text{ J m}^{-3} \text{ K}^{-1}$  (WRF\_CAP1) and  $7.5 \times 10^6 \text{ J m}^{-3} \text{ K}^{-1}$  (WRF\_CAP2). Finally, two LES(s) are initialized by using the WRF\_ALL and WRF\_CAP2 outputs.

The results of all these experiments are discussed in the next section, except for the LES experiment discussed in Sect. 3.4. Table 3 summarizes the main thermal and physical parameters (default values and following variations, in bold) used in the simulations discussed in the present paper.

## 3 Results and Discussion

### 3.1 Control Configuration

#### 3.1.1 Urban Area

In what follows, the WRF\_CNTR wind field and near-surface air temperature are compared with measurements of wind intensity and direction collected at the RM-L station (Fig. 4). The comparison is performed by interpolating the model output at the station level (20 m above ground level, a.g.l.). To the aim of verifying both the trend of the parameters near the ground and within the PBL, Fig. 5 shows the comparison between WRF and sodar vertical profiles of wind speed and direction at APL. This comparison allows for verifying the WRF ability to correctly simulate the vertical transport of momentum.

During the central hours of the day, WRF overestimates the wind speed (Fig. 4a) and correctly reproduce the wind direction (Fig. 4b), whereas between 1600 and 0900 UTC, a slight underestimation of the wind speed is found. During night-time, a small underestimation of the wind speed is found ( $0.5 \text{ m s}^{-1}$ ) probably caused by numerical and instrumental errors. Unfortunately, the measurement errors are not available; therefore it is not possible to estimate their weight. The time series of the simulated air temperature for WRF\_CNTR shows an underestimation with respect to the observations during the whole period (Fig. 4c, black and red lines, respectively), except for the maximum of the first day, which is very well reproduced. The maximum difference of  $4 \text{ }^\circ\text{C}$  is found during night-time at 0400 UTC.

The vertical profiles of horizontal wind velocity (Fig. 5a, b, sodar and WRF\_CNTR, respectively) and direction (Fig. 5c, d, sodar and WRF\_CNTR, respectively) depict a delay in the model results. On the other hand, WRF\_CNTR correctly reproduces the alternation of the sea breeze during daytime (wind blowing from south-west) and the land breeze during night-time (north-easterly wind). Moreover, WRF overestimates the wind intensity and the transport of momentum in the lowest layers of the atmosphere during 28 June, as already found by Pichelli et al. (2014), whereas the model underestimates the wind speed above the surface (500 m) during daytime on 29 June. The different behaviour of WRF during 28 and 29 June is very likely related to the different forcing of these days: 28 June is characterized

**Table 3** Default and modified values of thermal and physical parameters used in WRF for the simulations presented here

Parameter	WRF_CNTR	WRF_CAP	WRF_COND	WRF_ALB	WRF_EMS	WRF_ALL	WRF_ALB1	WRF_ALB2	WRF_CAP1	WRF_CAP2
CAPR (J m <sup>-3</sup> K <sup>-1</sup> )	1.0 × 10 <sup>6</sup>	<b>2.1 × 10<sup>6</sup></b>	1.0 × 10 <sup>6</sup>	1.0 × 10 <sup>6</sup>	1.0 × 10 <sup>6</sup>	<b>2.1 × 10<sup>6</sup></b>	<b>2.1 × 10<sup>6</sup></b>	<b>2.1 × 10<sup>6</sup></b>	<u>5.0 × 10<sup>6</sup></u>	<u>7.5 × 10<sup>6</sup></u>
CAPB (J m <sup>-3</sup> K <sup>-1</sup> )	1.0 × 10 <sup>6</sup>	<b>2.1 × 10<sup>6</sup></b>	1.0 × 10 <sup>6</sup>	1.0 × 10 <sup>6</sup>	1.0 × 10 <sup>6</sup>	<b>2.1 × 10<sup>6</sup></b>	<b>2.1 × 10<sup>6</sup></b>	<b>2.1 × 10<sup>6</sup></b>	<u>5.0 × 10<sup>6</sup></u>	<u>7.5 × 10<sup>6</sup></u>
CAPG (J m <sup>-3</sup> K <sup>-1</sup> )	1.4 × 10 <sup>6</sup>	<b>2.1 × 10<sup>6</sup></b>	1.4 × 10 <sup>6</sup>	1.4 × 10 <sup>6</sup>	1.4 × 10 <sup>6</sup>	<b>2.1 × 10<sup>6</sup></b>	<b>2.1 × 10<sup>6</sup></b>	<b>2.1 × 10<sup>6</sup></b>	<u>5.0 × 10<sup>6</sup></u>	<u>7.5 × 10<sup>6</sup></u>
AKSR (J s <sup>-1</sup> K <sup>-1</sup> )	0.67	0.67	<b>2.28</b>	0.67	0.67	<b>2.28</b>	<b>2.28</b>	<b>2.28</b>	<b>2.28</b>	<b>2.28</b>
AKSB (J s <sup>-1</sup> K <sup>-1</sup> )	0.67	0.67	<b>2.28</b>	0.67	0.67	<b>2.28</b>	<b>2.28</b>	<b>2.28</b>	<b>2.28</b>	<b>2.28</b>
AKSG (J s <sup>-1</sup> K <sup>-1</sup> )	0.4004	0.4004	<b>0.7</b>	0.4004	0.4004	<b>0.7</b>	<b>0.7</b>	<b>0.7</b>	<b>0.7</b>	<b>0.7</b>
ALBR (fraction)	0.20	0.20	0.20	<b>0.12</b>	0.20	<u><b>0.12</b></u>	<u><b>0.65</b></u>	<u><b>0.28</b></u>	<b>0.12</b>	<b>0.12</b>
ALBB (fraction)	0.20	0.20	0.20	<b>0.12</b>	0.20	<u><b>0.12</b></u>	<u><b>0.60</b></u>	<u><b>0.28</b></u>	<b>0.12</b>	<b>0.12</b>
ALBG (fraction)	0.20	0.20	0.20	<b>0.12</b>	0.20	<u><b>0.12</b></u>	<u><b>0.45</b></u>	<u><b>0.28</b></u>	<b>0.12</b>	<b>0.12</b>
EPSR (fraction)	0.90	0.90	0.90	0.90	<b>0.97</b>	<b>0.97</b>	<b>0.97</b>	<b>0.97</b>	<b>0.97</b>	<b>0.97</b>
EPSB (fraction)	0.90	0.90	0.90	0.90	<b>0.97</b>	<b>0.97</b>	<b>0.97</b>	<b>0.97</b>	<b>0.97</b>	<b>0.97</b>
EPSG (fraction)	0.95	0.95	0.95	0.95	<b>0.97</b>	<b>0.97</b>	<b>0.97</b>	<b>0.97</b>	<b>0.97</b>	<b>0.97</b>

The values modified with respect to the default configuration are shown in bold. The values underlined and in bold are the parameters further modified for WRF\_ALL in the simulations aimed at evaluating the effect of albedo and heat capacity

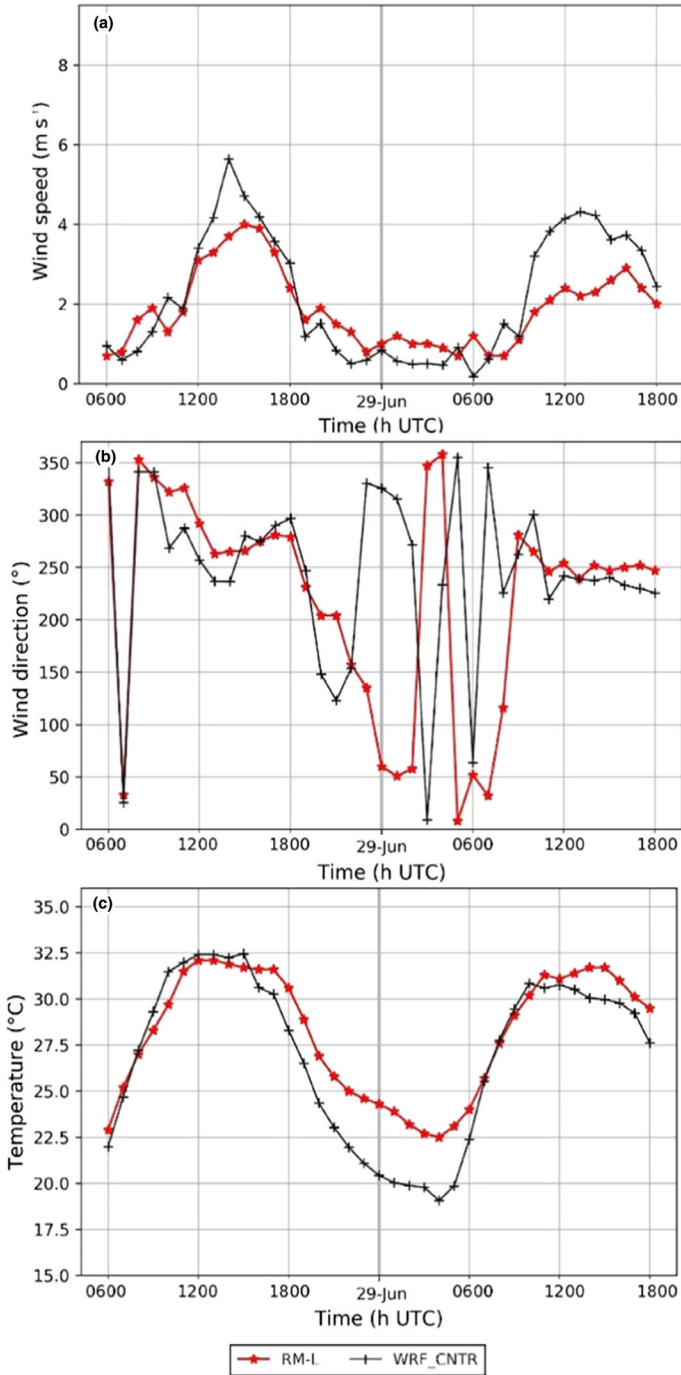


**Fig. 4** Time series of **a** wind speed, **b** wind direction, and **c** air temperature measured at RM-L station (red line) and simulated in WRF\_CNTR (black line)

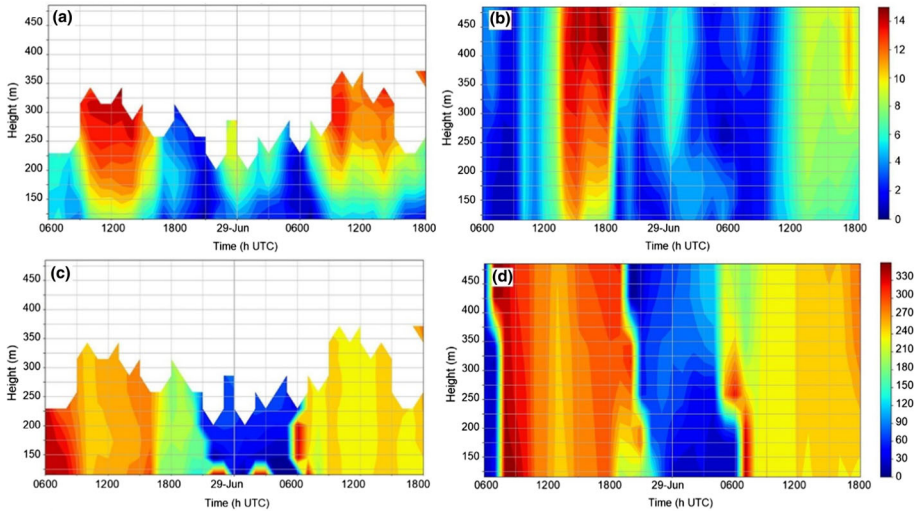


**Fig. 5** Vertical profile of wind speed [ $\text{m s}^{-1}$ ] from a sodar and b WRF\_CNTR and vertical profiles of wind direction [ $^{\circ}$ ] from c sodar and dWRF\_CNTR

by local forcing, whereas the large-scale forcing is driving on 29 June. It is well known that weak local forcings are more difficult to reproduce than the large-scale ones, which are driving the model through the initial and boundary conditions.

On 28 June, WRF produces a maximum wind speed of approximately  $12\text{--}14 \text{ m s}^{-1}$  at the lowest levels ( $125\text{--}175 \text{ m a.g.l.}$ ) at 1500 UTC, whereas the maximum wind speed recorded by the sodar at noon at the same level ranges from  $6$  to  $10 \text{ m s}^{-1}$ . The overestimation of the momentum transport from upper to lower layers is an indication of the WRF model being unable to decouple the canopy layer from the free atmosphere. Hence, from 1500 UTC, the overestimation of wind speed at lower layers results in a larger decreasing rate of air temperature in the afternoon (Fig. 4c), being that the upper layers are generally cooler than the lower ones. Yet, WRF\_CNTR misses the maximum values of wind velocities recorded by the sodar in the PBL (about  $8\text{--}14 \text{ m s}^{-1}$ ) during 28 June. As already discussed, the tendency of the model to bring high wind speed to lower levels can lead to negative feedback on the estimation of temperature values, especially at night, preventing WRF\_CNTR to correctly reproduce the UHI effect.

### 3.2 Model Sensitivity to Urban Parameters

Based on the previous results, BEP urban parameters are modified to improve the model ability to reproduce the nocturnal temperature trend in the metropolitan area. This exercise will also allow us to better understand the role of the urban parameters themselves.

In what follows, the different subsections present the results of the numerical simulations performed by varying several variables in WRF\_CNTR. The comparison between MODIS (WRF\_CNTR) and CORINE (WRF\_CORINE) allows us to evaluate the influence of the land use classification. The comparison shows that CORINE reproduces the UHI in Rome better than MODIS and that the advection of the breeze in the city centre is close to the observations. Hence, the impact of the urban thermal and geometric parameters is tested by a sensitivity

study carried out by varying the heat capacity, the thermal conductivity, the emissivity, and the albedo. This ends up in setting the configuration that better reproduces the circulation in the centre of Rome and the UHI. The comparison with the RM\_L station is performed by interpolating the model output at the sensor level (20 m a.g.l).

### 3.2.1 Land Use

To improve both the model simulation of the urban area and to highlight the differences between urban and rural areas, the first change concerns the land use categorization. The CORINE land use dataset is implemented because of its higher spatial resolution (100 m), the results show remarkable differences, even using the default BEP parameters (hereinafter, namely WRF\_CORINE). At RM-L, WRF\_CORINE is able to correctly reproduce the wind speed (Fig. 6a) during the daytime for 28 June, whereas during the night some discrepancies are still evident. During 29 June, the agreement decreased and the results for WRF\_CORINE are similar to WRF\_CNTR. The wind direction is very well reproduced on 28 June (Fig. 6b), whereas the results deteriorate at night and on 29 June. Moreover, no differences are found for the air temperature (Fig. 6c): WRF\_CNTR and WRF\_CORINE are very similar and differ only in the final hours of the simulation. During daytime, the temperature is well reproduced, whereas the night minimum is still strongly underestimated. Vertical profiles of wind speed and direction (not shown) highlight a good estimation of wind speed, especially at high levels on 29 June, whereas the onset of the sea breeze still shows a delay for WRF\_CORINE. Moreover, an overestimation of the momentum transport from higher to lower levels (not shown) is still found. Therefore, the impact of the high-resolution land use on the temperature is found very small, whereas the wind field is positively affected.

### 3.2.2 Thermal and Physical Parameters

In what follows, the CORINE land use is used (WRF\_CORINE) for all the experiments, while the BEP urban variables and the thermal and physical parameters involved in the metropolitan characterization are modified.

As first, the urban parameters are optimized for Rome, according to Morini et al. (2018). Then, the WRF\_CAP, WRF\_COND, WRF\_ALB, and WRF\_EMS simulations (details in Table 3) are carried out, changing one by one the heat capacity, the thermal conductivity, the albedo, and the emissivity of roofs, buildings, and ground, respectively. The values are modified according to similar urban configurations (e.g. Sugawara and Takamura 2014; Falasca and Curci 2018, see Sect. 2.3 for details). Figure 7a, b shows the comparison of wind speed and direction among WRF\_CORINE, the simulations obtained by modifying the various urban parameters, and the measurements at RM-L. All simulations show an overall similar trend: good agreement until sunset on 28 June, underestimation of the wind speed at night, and a worsening of the results on 29 June. Nevertheless, any simulation shows that the onset of the breeze is well captured by all set-ups, except for WRF\_ALB, which anticipates the increase in wind intensity and postpones the change in the wind direction by an hour. During the night, according to the land breeze regime a northerly wind is found, causing a marked oscillation around the north direction. In particular, WRF\_ALL and WRF\_CAP are the ones that better reproduce the in situ measurements. During the day, the WRF\_ALL temperature time series (Fig. 7c) closely follows the observations and correctly reproduces the morning temperature increase and the daily maximum (about 32 °C at 1300 UTC). On the other hand, all simulations anticipate the afternoon cool-down by approximately three hours,

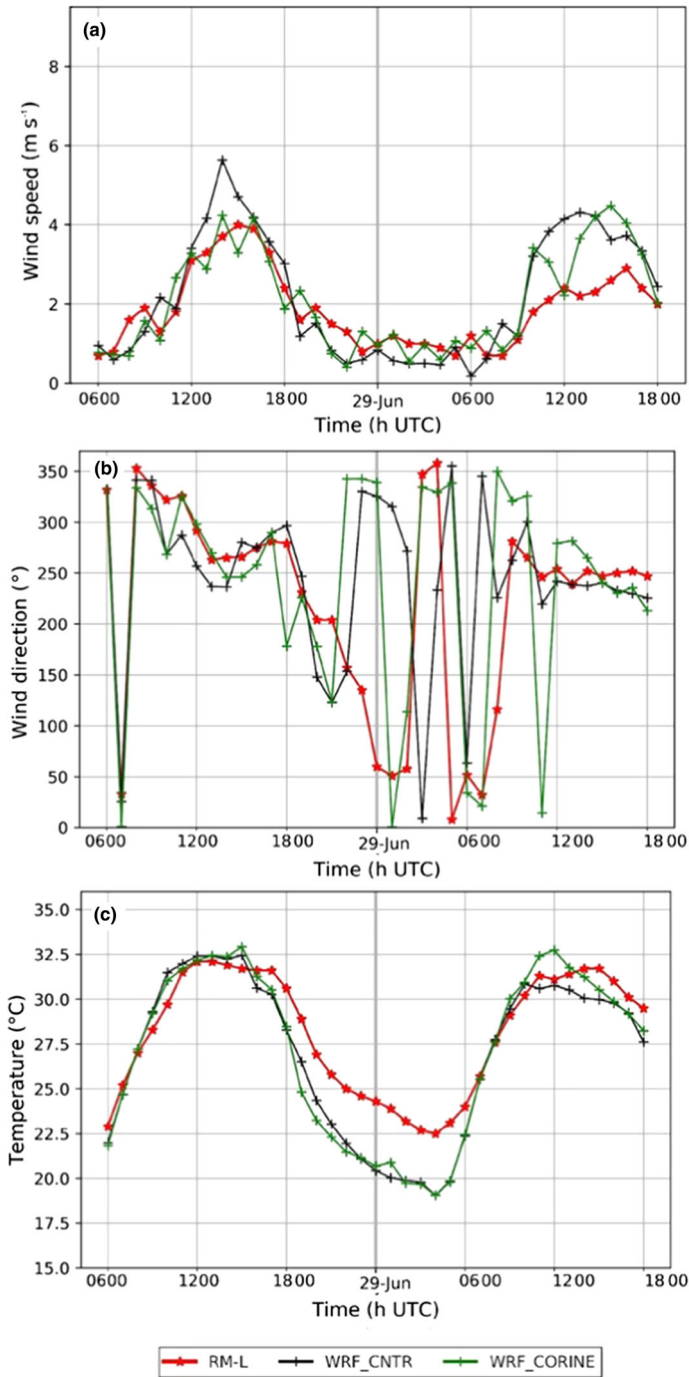


**Fig. 6** Time series of **a** wind speed, **b** wind direction, and **c** air temperature measured at RM-L station (red line) and simulated in WRF\_CNTR (black line) and WRF\_CORINE (green line)

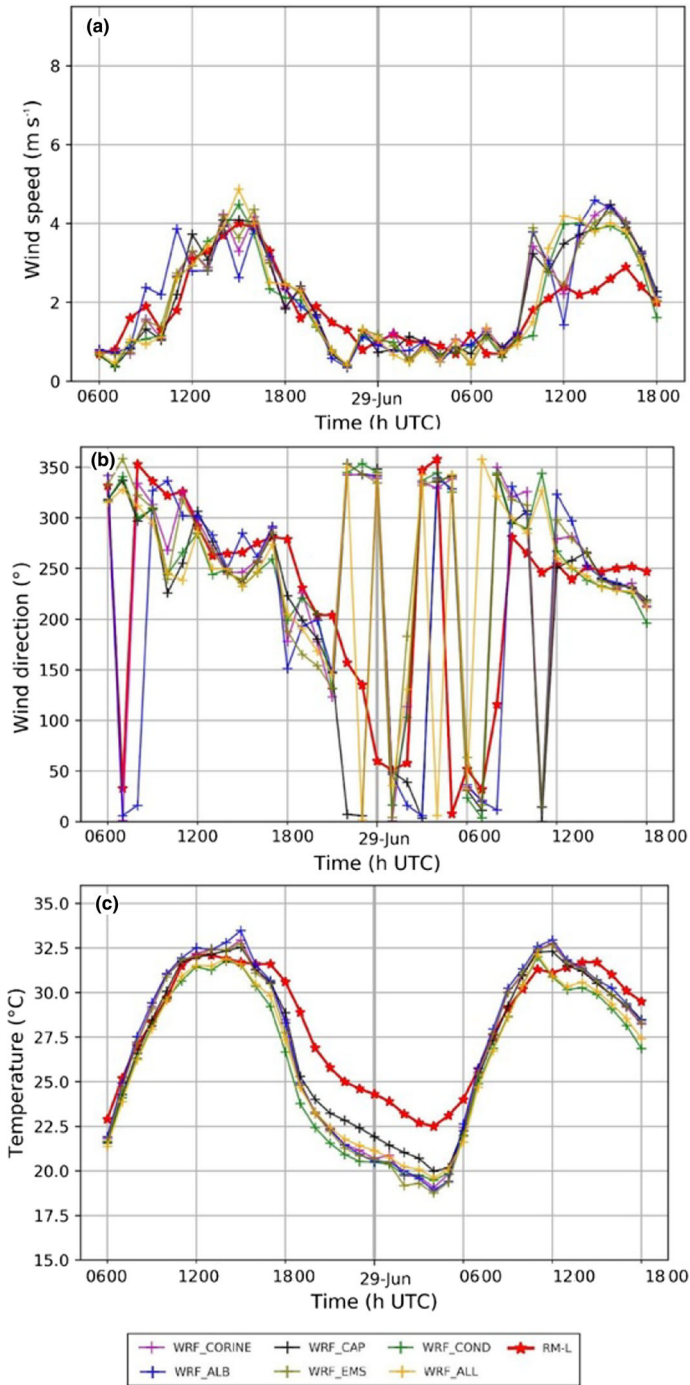


**Fig. 7** Time series of **a** wind speed, **b** wind direction, and **c** air temperature measured at RM-L station (red line) and simulated changing thermal and physical urban parameters



worsening the night trend. Therefore, a general WRF difficulty to reproduce the UHI at night is found: all simulations underestimate the observed temperature with a maximum difference between 3.5 °C (WRF\_EMS) and 2.5 °C (WRF\_CAP) at 0400 UTC. Again, on 29 June, after the sunrise, the increase in temperature due to the solar radiation is well reproduced.

In summary, the results of the previous experiments suggest that the optimization of BEP results only in slight improvements, while difficulties in correctly reproducing the night-time temperature and the UHI are still found. The previous discussion suggests that the albedo and the heat capacity largely influence the model ability in reproducing the ground variables. The key role of heat capacity and albedo for the temperature evolution is well-known (Sharma et al. 2014): the former is responsible for the release of nocturnal heat, controlling the evening and night temperature, while the latter is one of the main diurnal forcing, as it determines the amount of heat absorbed by the urban area. For this reason, albedo and heat capacity, already changed in WRF\_ALL, are further modified to investigate the model sensitivity to them.

### 3.2.3 Sensitivity Analysis on Albedo

Two simulations are carried out to evaluate the sensitivity of WRF to the albedo: in the former (WRF\_ALB1)  $ALBR = 0.65$ ,  $ALBB = 0.60$ ,  $ALBG = 0.45$  are set, in the latter (WRF\_ALB2), the three albedo values are equal to 0.28.

The time series of wind speed and direction (Fig. 8a, b, respectively) and temperature (Fig. 8c) show that WRF is sensitive to the albedo. Large differences between WRF\_ALB1 and the urban measurements are observed: the maximum daily value of wind intensity is underestimated by 40% on 28 June, whereas all the simulations underestimate and overestimate the measurements during night-time 28 and on 29 June, respectively. In addition, the wind direction deteriorates when the albedo increases. The air temperature trend worsens during the day by increasing the albedo, whereas at night there are no substantial changes in the model results, with a general underestimation of 2.5 °C (about 12%). This suggests that the increase in albedo does not improve the agreement between the model meteorological parameters and the real urban conditions.

As a preliminary conclusion, these results suggest that the most representative albedo value for the urban area of Rome, among those discussed, is 0.12. Such a value is higher than the ones reported in the literature (Offerle et al. 2003) but in agreement with experimental findings in Rome (Sozzi et al. 2020). Indeed, the authors reported a zenith angle albedo of 0.30, hence, the comparison must be carried out by adding the values found in the present paper for roofs, buildings, and ground, obtaining a total value of 0.36.

### 3.2.4 Sensitivity Analysis on Heat Capacity

The WRF\_CAP1 and WRF\_CAP2 experiments are performed by increasing the heat capacity up to  $5.0 \times 10^6 \text{ J m}^{-3} \text{ K}^{-1}$  and to  $7.5 \times 10^6 \text{ J m}^{-3} \text{ K}^{-1}$ , respectively. As shown in Fig. 9a, b, the increase in heat capacity does not produce substantial improvements in wind speed and direction. On the contrary, the underestimation of the temperature during night-time is considerably reduced (Fig. 9c), with a maximum difference that decreases to approximately 3.5 °C (WRF\_ALL) and 0.8 °C (WRF\_CAP2).

Thus, these results show that WRF\_ALL still misses the nocturnal minimum, which is well reproduced varying the heat capacity (WRF\_CAPs). This suggests a better ability to reproduce the local circulation of the urban area than the other configurations. Moreover, difficulties are found in reproducing either the diurnal temperature and/or the local circulation.

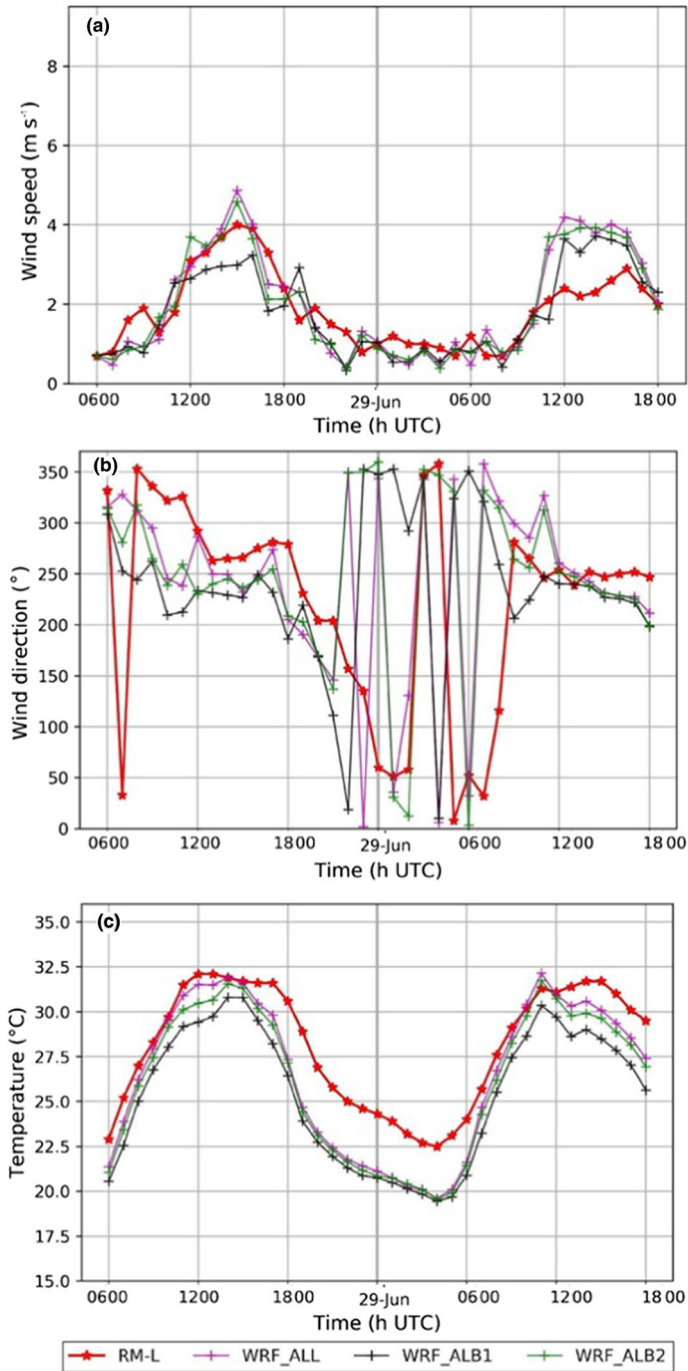


**Fig. 8** Time series of **a** wind speed, **b** wind direction, and **c** air temperature measured at RM-L station (red line), simulated in WRF\_ALL (magenta line), setting  $ALBR = 0.65$ ,  $ALBB = 0.60$ ,  $ALBG = 0.40$  (WRF\_ALB1, black line) and  $ALBR = ALBB = ALBG = 0.40$  (WRF\_ALB2, green line)

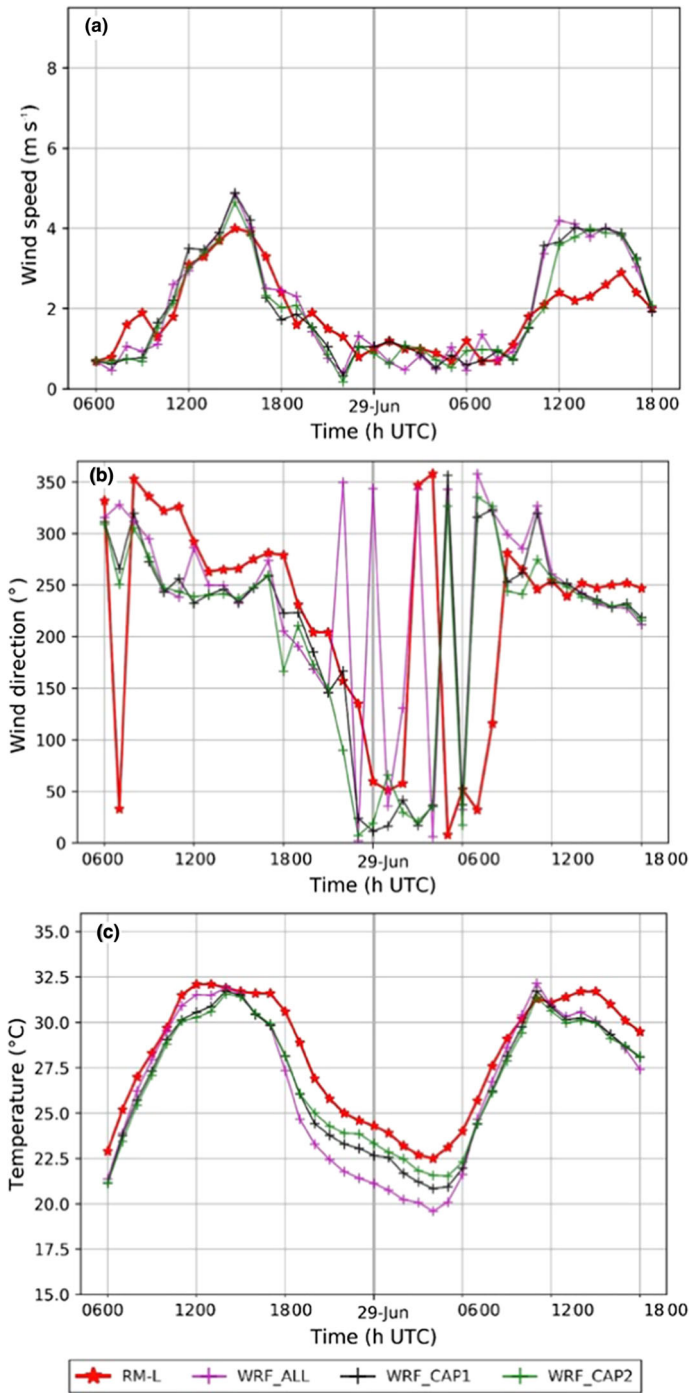


**Fig. 9** Time series of **a** wind speed, **b** wind direction, and **c** air temperature measured at RM-L station (red line) and simulated varying the heat capacity to  $5.0 \times 10^6 \text{ J m}^{-3} \text{ K}^{-1}$  (WRF\_CAP1, black line) and  $7.5 \times 10^6 \text{ J m}^{-3} \text{ K}^{-1}$  (WRF\_CAP2, green line)

**Table 4** Correlation coefficient for air temperature and wind speed between WRF simulations and observations at RM-L station

	Correlation coefficient		RMSE
	Air temperature	Wind speed	Air temperature
WRF_CNTR	0.960	0.863	/
WRF_CORINE	0.959	0.824	/
WRF_CAP	0.976	0.861	/
WRF_COND	0.950	0.831	/
WRF_ALB	0.956	0.735	/
WRF_EMS	0.959	0.835	/
WRF_ALL	0.970	0.841	1.960
WRF_ALB1	0.970	0.739	2.741
WRF_ALB2	0.970	0.831	2.169
WRF_CAP1	0.986	0.855	1.349
WRF_CAP2	0.986	0.850	1.222

The RMSE for air temperature is computed only for the last 4 simulations

This is probably caused by the too coarse resolution used for the investigation. Based on this hypothesis, further investigation is performed using LES at a resolution of 111 m, initialized using the best initial condition produced by the WRF simulations. To the aim of objectively comparing the WRF simulations two statistical indicators are used: the correlation coefficient and the root-mean-square error (RMSE). Moreover, the statistical evaluation is carried out considering only the observations acquired in the downtown Rome (i.e. the RM-L weather station) because the investigation is focused on this area. Thus, the evaluation has no statistical significance, and it is only an objective comparison.

### 3.2.5 Correlation Coefficient and Root-Mean-Square Error

The correlation coefficients for temperature and wind speed and the RMSE for temperature only are shown in Table 4: large values, ranging between 0.95 (WRF\_COND) and 0.98 (WRF\_CAPs) are found for the correlation coefficient for temperature, with the smallest values produced by WRF\_COND. This suggests that the chosen values for the building conductivity are not improving the model results with respect to WRF\_CNTR in the urban area. On the other hand, the WRF heat capacity experiments produce the largest correlation coefficient, suggesting a strong sensitivity of WRF to this parameter. Also, the albedo experiments, as well as WRF\_ALL, show a large correlation coefficient for temperature. The wind speed correlation coefficients show a large value as well, ranging between 0.73 (WRF\_ALB) and 0.86 (WRF\_CNTR) but slightly smaller than the one for temperature, which is normally higher because of the temperature daily cycle. The RMSE for temperature could help differentiate among the WRF\_CAPs, WRF\_ALBs, and WRF\_ALL experiments. The RMSE values clearly show differences among these simulations with values ranging between 1.22 (WRF\_CAP2) and 2.74 (WRF\_ALB2), which allows us to conclude that WRF\_CAP2 is the simulation with the lowest RMSE and the highest correlation coefficient. Therefore, the WRF\_CAP2, together with WRF\_ALL outputs, are used to initialize the LES(s) presented in the following section.

### 3.3 Analysis of the Circulation in the Urban–Rural Area

In what follows, an investigation of the circulation generated by the interaction of the sea-breeze front with the urban area in its propagation inland is presented. This investigation is twofold: (i) to analyse the changes of the breeze front going inland and vice versa, and (ii) to examine the effect of the interaction between breeze regime and urban area. To better understand these issues, the two best simulations are used: both WRF\_ALL and WRF\_CAP2 output are compared with measurements collected by rural in situ stations, selected in the surroundings of Rome. The comparison with the surface stations is performed retrieving the WRF wind speed at 2 m a.g.l. by using a log-profile, while for the wind direction the 10 m a.g.l. values are used. The temperature comparison is performed at 2 m a.g.l.

Several transects, using stations approximately aligned along the coast-inland section, are built and analysed to investigate the evolution of the momentum flux, but only the most meaningful is presented here, i.e. the one normal to the coastline passing through the city centre. This transect includes, from the coast to the hinterland, the ARSIAL stations of Capracotta (RM-C), Roma–Lanciani (RM-L), Monterotondo (MR), and Montelibretti (ML), as depicted in Fig. 2b. At the RM-C station (on the seaside), the model well reproduces the sea-breeze regime, catching the changes in wind intensity and direction, but with an overestimation of the wind speed (Fig. 10a, b) during 28 June for both simulations. Moreover, a small underestimation of the first day maximum of the temperature, together with an overestimation of the minimum, is found (Fig. 10c) for both simulations. During 29 June, the underestimation of the temperature maximum is larger than during the previous day. As the sea-breeze front reaches the urban area, the wind field shows a larger variability than at RM-C as shown by the wind direction (Fig. 10e); on the other hand, the wind speed is very well reproduced during 28 June (Fig. 10d). Finally, the temperature time series is much better reproduced for both the maxima and the minimum (Fig. 10f) than along the coast (RM-C). Noteworthy, the night-time temperature minimum is well reproduced by WRF\_CAP2, suggesting a key role for the conductivity to correctly reproduce the temperature trend. The sea-breeze front is detectable from the change in wind direction and it can still be found at MR (inland, east of the urban area, Fig. 10h), but a larger variability is simulated during night-time. On the contrary, the model reproduced very well both the wind speed and temperature at MR (Fig. 10g,i, respectively). As the sea breeze front moves further inland, the model ability decreases. In fact, the wind speed (Fig. 10j) is largely overestimated (about  $7 \text{ m s}^{-1}$ ), the wind direction is noisy (Fig. 10k) and the night-time minimum for the temperature (Fig. 10l) is largely overestimated at ML. The model reaches  $20.0 \text{ }^\circ\text{C}$  and  $21.0 \text{ }^\circ\text{C}$  (respectively for WRF\_ALL and WRF\_CAP2), whereas the station temperature is below  $17.5 \text{ }^\circ\text{C}$ . In summary, the previous analysis allows for asserting that WRF can correctly reproduce the onset of the breeze regime (sea and land) and the daily temperature variation. As the sea breeze front proceeds inland, the model ability to simulate wind speed and direction decreases and temperature minimum at night-time in the urban area is not correctly reproduced. The smooth rate of temperature decrease turns into an underestimation of night-time minimum in the suburban areas, suggesting that the impact of the city on the atmospheric parameters is not correctly simulated.

### 3.4 Large-Eddy Simulations

To further investigate the local circulation in the urban area, the previous two best simulations (WRF\_ALL and WRF\_CAP2) are used to force two LES(s) using outputs at the closest coarse

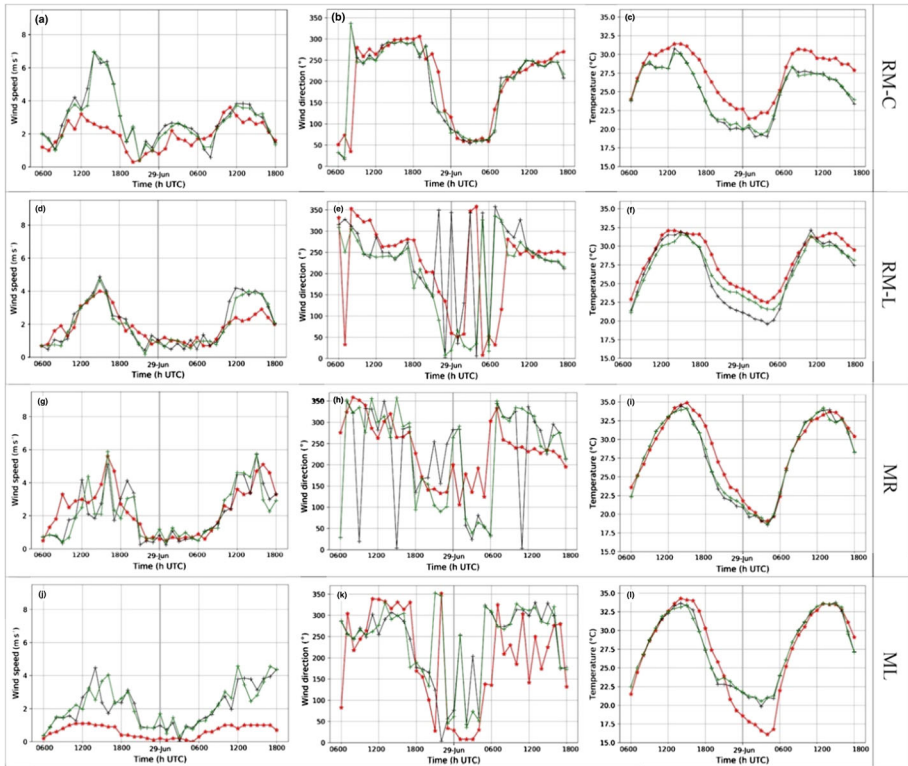


**Fig. 10** Time series of wind speed (a, d, g and j), wind direction (b, e, h and k), and temperature (c, f, i and l) measured (red lines) and simulated by WRF\_ALL (black lines) and WRF\_CAP2 (green lines) at RM-C (a, b, c), RM-L (d, e, f), MR (g, h, i), and ML (j, k, l)

resolution (1 km). A two-way nesting structure using D2, D3, and D4, as shown in Fig. 2a, b, is used for the LES; domains D3 and D4, with a spatial resolution of 333 m and 111 m, respectively, have been added to D2. To the aim of correctly resolving the PBL, 80 hybrid vertical levels are used, with a higher resolution toward the ground and the first model level set at 25 m a.g.l, to avoid model instability. The same settings of the previous simulations are used, but the physical processes in the PBL are explicitly resolved in the two innermost domains using a three-dimensional TKE subgrid model (Deardorff 1980) (Table 5). For the sake of brevity, only the results obtained starting from WRF\_CAP2 are shown. Hereinafter, the WRF\_CAP2 simulation is named NO-LES WRF\_CAP2.

To investigate the role of the high resolution into the characterization of the circulation in Rome, a comparison between LES and RM-L station is also presented. The maximum wind speed by LES is associated with the entering of the sea breeze front, correctly capturing the onset of the breeze as shown by the change in wind direction (Fig. 11b). Nonetheless, the wind speed is overestimated (Fig. 11a). However, it is worth noting that, at a very high resolution, the point-by-point comparison can largely penalize the model results because of the heterogeneity of the urban environment, the error in the position of the wind maximum/minimum, and the lack of high resolution network of measurements. This would explain the overestimation of the wind speed between 1500 and 1800 UTC, when the horizontal wind variation

**Table 5** List of physical parameterizations used for different domains in LES(s)

Physics options	D2	D3	D4
Microphysics	WSM6	WSM6	WSM6
Longwave radiation	RRTM	RRTM	RRTM
Short wave radiation	Dudhia	Dudhia	Dudhia
PBL	MYJ	Explicitly solved	Explicitly solved
Land surface physics	Noah LSM	Noah LSM	Noah LSM

is large (not shown). Also, the nocturnal jet is overestimated as well as the maximum wind speed during the second day. The trend of the diurnal temperature is improved compared to the NO-LES WRF simulation: the decreasing rate of temperature after noon is very well reproduced (Fig. 11c) as well as the minimum, but a slight underestimation of the nocturnal minimum is still found. Similar results are found for the simulation performed using the WRF\_ALL initialization, suggesting that the LES physics is driving these results more than the initial conditions.

Moreover, the correlation coefficients for temperature, wind speed at the first model eta level, and the RMSE for the temperature are also estimated. Good correlation coefficient and RMSE values for air temperature (0.978 and 1.082, respectively) and a lower correlation coefficient for wind speed (0.567) than in the coarse resolution configuration are obtained.

To investigate the structure of the circulation in the urban area, the spatial distribution of wind speed at 10 m a.g.l., together with the temperature at 2 m a.g.l., is also discussed by comparing the LES and NO-LES WRF\_CAP2 simulations. In what follows, the horizontal fields at 1000 UTC, 1200 UTC, and 1400 UTC are selected (Fig. 12), for analysing the sea breeze front development, its inland propagation, and its interaction with the city.

The surface temperature and the horizontal wind structure clearly show the interaction of the urban area with the sea breeze, whereas the horizontal wind is undisturbed at 975 hPa (not shown) and the sea breeze flow crosses over the entire area of Rome. At 10 m a.g.l., the LES shows the sea breeze front reaching the boundary of Rome approximately at 1000 UTC (Fig. 12a, black circle), identifying three different wind directions: (i) a west component in the western flank of the city (i.e. close to the sea); (ii) a north-west component in the northern region (i.e. the inland side), and (iii) a south-west component in the southern portion of the city. The NO-LES WRF\_CAP2 simulation shows a structure similar to LES at this time (Fig. 12b). At noon, LES (Fig. 12c) shows an increase in the sea breeze due to the convergence between north-west and the south-west components, especially in the west-north-west flank. Moreover, entering the urban area, the flow splits in a southern and a northern flank (Fig. 12c), reinforcing the south-west component in the southern side of the city. This result agrees with Di Bernardino et al. (2021), who used surface remote sensing measurements to show the persistence of a south-west component of the sea breeze in downtown Rome. At the same time, the NO-LES WRF\_CAP2 simulation (Fig. 12d) shows a different structure for both temperature and horizontal wind. The temperature increases in the inner part of the city, and the wind speed increases without splitting as it enters the urban area. Finally, at 1400 UTC, the north branch of the flow is almost completely damped, whereas an increase in the southern flank is found for LES (Fig. 12e). The 2-m temperature shows a structure compatible with

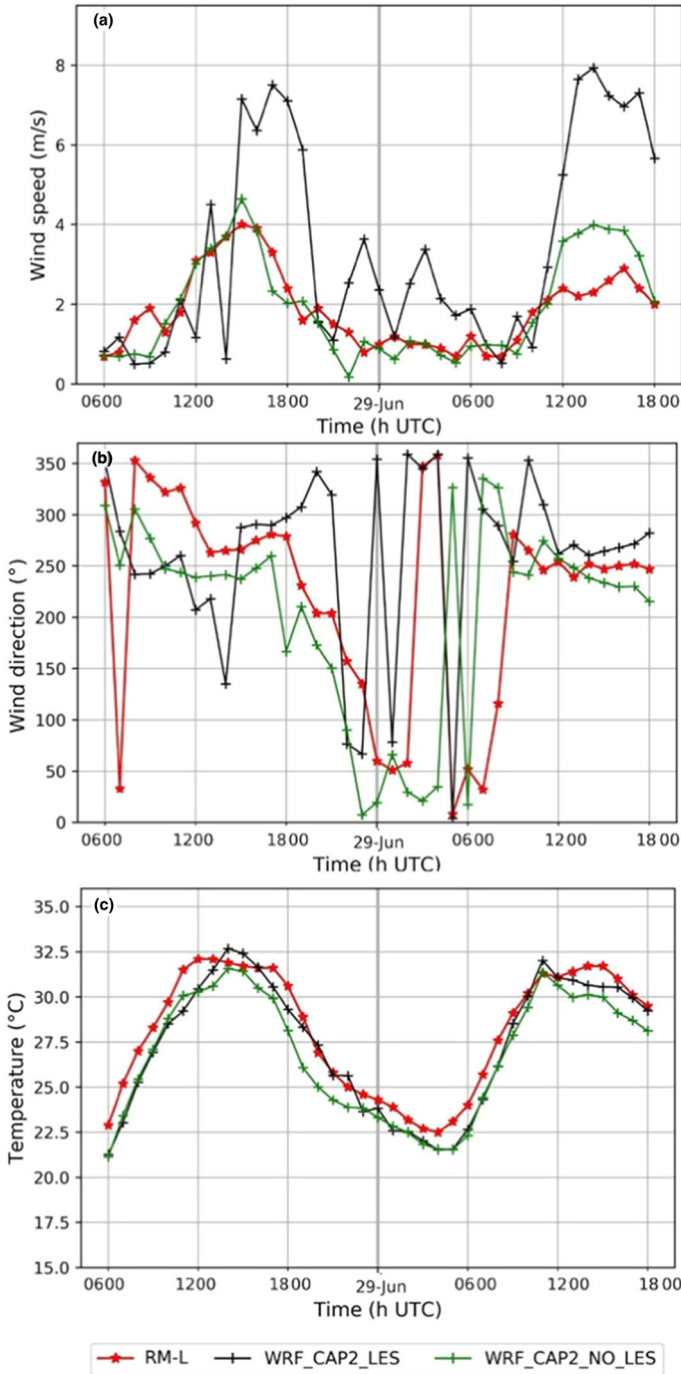


**Fig. 11** Time series of **a** wind speed, **b** wind direction, and **c** air temperature measured at RM-L station (red line) and obtained by the NO-LES WRF\_CAP2 (green line) and LES(s) (black line)



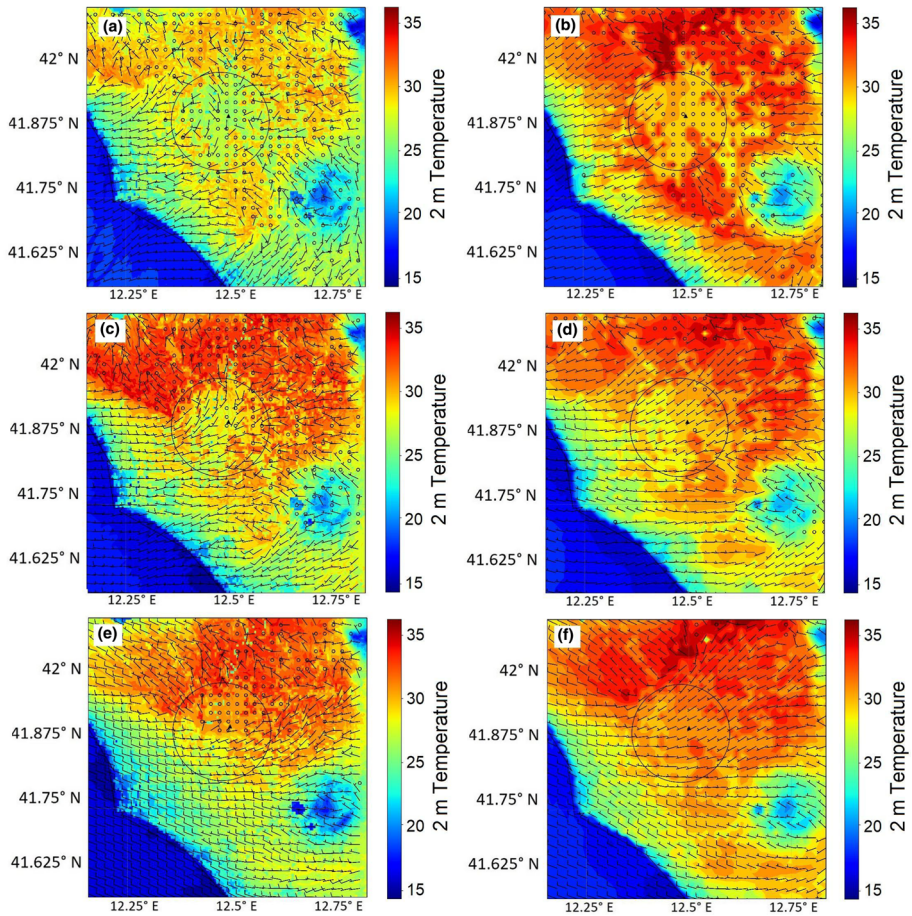


**Fig. 12** Air temperature (colors) at 2 m a.g.l. and horizontal velocity (barbs) at 10 m a.g.l. for 28 June 2011 at 1000 UTC (a) and (b), 1200 UTC (c) and (d), and 1400 UTC (e) and (f). Left column: LES. Right column: NO-LES WRF\_CAP2

the wind regime: low temperature values in the west flank caused by the wind effect, and high temperatures in the east flank caused by the calm wind conditions (Fig. 12e). On the other hand, the NO-LES WRF\_CAP2 simulation shows different wind and 2-m temperature fields (Fig. 12f): the wind enters the urban area undisturbed, and the temperature increase is not at all reduced by the wind. Furthermore, as highlighted in Fig. 12a, b, if calm wind occurs, the urban area can experience temperatures lower than the surrounding rural areas. A possible explanation of this behaviour is the building shadow effect, which reduces the daytime temperatures due to the reflection of radiation (Zhang et al 2017; Lian et al. 2018). The presence of tall buildings in downtown Rome can block the solar radiation and can cast shadows, slowing down the heat energy accumulation and its transition into the atmosphere. This aspect, in contrast to what was expected in the case of UHI, is still under investigation and will be explored in further studies.

The strong interaction between UHI and the sea breeze shown by LES is probably responsible for the wind and temperature fields. Indeed, the cross sections taken inside the circle

delimiting the urban area of Rome (north–south and east–west, not shown) at 1400 UTC reveal strong plumes and downdrafts developing in the north-east sector. The increase in the surface heating triggers the plume development overwhelming the sea breeze flow and almost completely dumping the wind speed. The open question is why the sea breeze flow is dumped only on the northern side, while the south-west component is reinforced in the southern flank. Probably, this is due to the combination of two factors: the building density and the complex orography. Historically, the development of the city of Rome started in the north; hence, a possible explanation is a denser urban structure acting as a barrier to the sea breeze, whereas the patchy distribution of green areas in the southern side do not block the sea breeze front. In addition, there are several hills in the northside of Rome, whereas the south side is flat.

However, understanding this phenomenon is particularly complex. The combination of the surface heating generating plumes and the drag of the orography produces the split of the sea breeze, which turns in a convergence line, increasing the intensity of the south-west wind component. Consequently, the reinforced sea breeze front can enter undisturbed in the southern sector of the urban area of Rome. To support the LES findings, a few stations in the north-east, south-west, and east sectors are used (Fig. 2b). One of these stations is outside of the LES domain (ML, Fig. 2b) but close to the area under investigation; therefore, it is considered anyway. The MA, ML, and PA stations show wind speeds (Fig. 13, blue, olive green, and black lines, respectively) reaching  $1.0 \text{ m s}^{-1}$  (MA and ML) and  $1.6 \text{ m s}^{-1}$  (PA) between 1000 and 1400 UTC. These stations are located in the north-east rural area and their observations agree with the LES results at the same time (Fig. 12a, c, e). The stations located in the south-west and east sides, i.e. MN, MP, RM-P, and ZA (Fig. 13, magenta, red, brown, and yellow lines, respectively), show wind speeds ranging from 2 to  $3 \text{ m s}^{-1}$  at 1000 UTC, increasing up to  $3.5 \text{ m s}^{-1}$  at 1200 UTC and reaching a maximum of about  $4 \text{ m s}^{-1}$  at 1400 UTC. The wind speeds at the location of the stations are in good agreement with what is reproduced by LES (Fig. 12a, c, e).

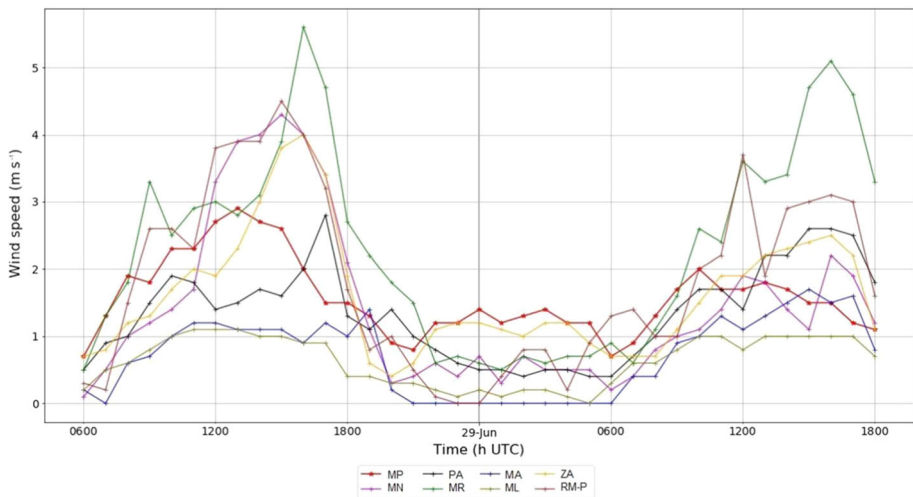


**Fig. 13** Time series of wind speed measured at MP (red), MN (magenta), PA (black), MR (green), MA (blue), ML (olive green), ZA (yellow), and RM-P (brown)

In summary, the LES experiment highlights the strong interaction between the sea breeze and the UHI and the consequent peculiar structure of the wind field in the urban area. The UHI acts to both deflect and suppress the sea breeze, in the south and north sides of the city, respectively. On the other hand, NO-LES WRF\_CAP2 and WRF\_ALL are not able to capture this peculiar feature.

## 4 Conclusions

In the present study, The WRF model was used to investigate the local circulation in the urban area in Rome and its interaction with mesoscale and local phenomena, i.e. the sea breeze regime and the UHI. The model results are compared with the in situ observations of wind speed, wind direction, and temperature in the urban area and in its rural surroundings. Furthermore, the vertical profiles of wind speed and direction, measured in the Rome downtown, are used to evaluate the reproduction of vertical fluxes. All the simulations are performed using the BEP model and are compared with a control run, named WRF\_CNTR.

The results do not show a remarkable improvement in the temperature trend compared to WRF\_CNTR, although the CORINE dataset provides updated and more detailed land use data. On the contrary, the wind field shows improvement in the same area. The WRF\_CORINE set-up, together with the geometric, thermal, and physical parameters of the urban surfaces is changed based on previous works or using ad hoc estimations.

The optimization of the BEP parameters produces a moderately positive effect on the structure of the urban flux circulation, but large differences with the observations are still found at the night-time temperature. To improve this trend, a few further experiments are performed by changing the albedo and the heat capacity, i.e. the parameters mainly driving the temperature diurnal evolution. The best representation of the diurnal temperature cycle in the urban area is obtained by reducing the albedo for all the surfaces to 0.12. On the other hand, the tuning of the heat capacity suggests an improvement in reproducing the temperature, increasing the values of the surface heat capacity up to  $7.5 \times 10^6 \text{ J m}^{-3} \text{ K}^{-1}$  (WRF\_CAP2). In the latter case, the difference between the measured night temperatures and the numerical outputs is reduced to about 1.5 °C.

To further improve the model ability to reproduce the local circulation, two simulations are carried out in LES mode initialized using the WRF outputs that show the best agreement with urban observations at the closest coarse resolution (1 km). The daily temperature cycle shows a large improvement for LES, although the nocturnal jet is slightly overestimated as well as the wind speed maximum in the second part of the simulation. Thus, the diurnal variation of the temperature is improved with respect to the WRF runs, with a nocturnal underestimation of about 0.5 °C. Finally, LES captures the interaction between the local circulation and the onset of the sea breeze. The LES horizontal wind fields near the surface clearly show the onset of the breeze front, its propagation inland, and the interaction with the city. The latter effect generates three different wind branches associated with the front propagation: (i) a west component in the western flank of the city, closer to the sea; (ii) a north-west component in the northern, inland side, and (iii) a south-west component in the south area of the city. This separation of the wind field is probably due to two concurring factors: orography and anthropogenic activities. This latter phenomenon will be investigated in further studies.

A further interesting result revealed by LES is that, under calm wind conditions, the urban area of Rome can experience lower temperatures than the surrounding rural areas. This is

likely due to the shading of the tall urban buildings that can block sunshine and can cast shadows, slowing down the heat energy accumulation and its transition into the atmosphere. This result, in contrast to what is expected in the case of UHI, will be explored in further studies.

**Acknowledgements** The authors gratefully thank ARSIAL for providing meteorological data, Dr. Monica Campanelli and the BAQUNIN team for providing scientific and technical support in acquiring sodar profiles. CETEMPS and ECMWF are acknowledged for computer time and supporting this research. NCAR is acknowledged for the WRF code.

**Funding** Open access funding provided by Università degli Studi di Roma La Sapienza within the CRUI-CARE Agreement.

**Data availability** The datasets analysed during the current study are available in the <http://www.arsial> repository.

## Declarations

**Competing interests** The authors declare no competing interests.

**Open Access** This article is licensed under a Creative Commons Attribution 4.0 International License, which permits use, sharing, adaptation, distribution and reproduction in any medium or format, as long as you give appropriate credit to the original author(s) and the source, provide a link to the Creative Commons licence, and indicate if changes were made. The images or other third party material in this article are included in the article's Creative Commons licence, unless indicated otherwise in a credit line to the material. If material is not included in the article's Creative Commons licence and your intended use is not permitted by statutory regulation or exceeds the permitted use, you will need to obtain permission directly from the copyright holder. To view a copy of this licence, visit <http://creativecommons.org/licenses/by/4.0/>.

## References

- Bou-Zeid E, Meneveau C, Parlange MB (2004) Large-eddy simulation of neutral atmospheric boundary layer flow over heterogeneous surfaces: blending height and effective surface roughness. *Water Resour Res* 40:W02505
- Bryan G, Skamarock W, Rotunno R (2008) A conceptual framework for the resolution dependence of updraft properties in cloud system resolving models. *Eos Trans Am Geophys Union* 89:53 (Abstract A43G-07)
- Campanelli M, Siani AM, di Sarra A, Iannarelli AM, Sanò P, Diémoz H, Casasanta G, Cacciani M, Tofful L, Dietrich S (2019) Aerosol optical characteristics in the urban area of Rome, Italy, and their impact on the UV index. *Atmos Meas Tech* 15:1171–1183
- Casasanta G, Pietroni I, Petenko I, Argentini S (2014) Observed and modelled convective mixing-layer height at Dome C, Antarctica. *Boundary-Layer Meteorol* 151:597–608
- Chan PW (2009) Atmospheric turbulence in complex terrain: verifying numerical model results with observations by remote sensing instruments. *Meteor Atmos Phys* 103:145–157
- Chen F, Kusaka H, Bornstein R, Ching J, Grimmond CSB, Grossman-Clarke S, Loridan T, Manning KW, Martilli A, Miao S, Sailor D, Salamanca FP, Taha H, Tewari M, Wang X, Wyszogrodzki AA, Zhang C (2011) The integrated WRF/urban modelling system: development, evaluation, and applications to urban environmental problems. *Int J Climatol* 31(2):273–288
- Chen F, Yang X, Zhu W (2014) WRF simulations of urban heat island under hot-weather synoptic conditions: the case study of Hangzhou City, China. *Atmos Res* 138:364–377
- Ciancio V, Falasca S, Golasi I, Curci G, Coppi M, Salata F (2018) Influence of input climatic data on simulations of annual energy needs of a building: EnergyPlus and WRF modeling for a case study in Rome (Italy). *Energies* 11(10):2835
- Courault D, Drobinski P, Brunet Y, Lacarrere P, Talbot C (2007) Impact of surface heterogeneity on a buoyancy-driven convective boundary layer in light winds. *Boundary-Layer Meteorology* 124:383–403
- Deardorff JW (1980) Stratocumulus-capped mixed layers derived from a three-dimensional model. *Bound-Layer Meteor* 18:495–527

- Di Bernardino A, Iannarelli AM, Casadio S, Mevi G, Campanelli M, Casasanta G, Cede A, Tiefengraber M, Siani AM, Cacciani M (2021) On the effect of sea breeze regime on aerosols and gases properties in the urban area of Rome, Italy. *Urban Clim* 37:100842
- Dudhia J (1989) Numerical study of convection observed during the Winter Monsoon Experiment using a mesoscale two-dimensional model. *J Atmos Sci* 46:3077–3107
- EEA (2018) Corine Land Cover (CLC) 2018, Version 20b2. Release Date: 21–12–2018. European Environment Agency. <https://land.copernicus.eu/pan-european/corine-land-cover/clc2018>
- Falasca S, Curci G (2018) Impact of highly reflective materials on meteorology, PM10 and ozone in urban areas: a modeling study with WRF-CHIMERE at high resolution over Milan (Italy). *Urban Sci* 2(1):18
- Ferretti R, Lombardi A, Tomassetti B, Sangelantoni L, Colaiuda V, Mazzarella V, Maiello I, Verdecchia M, Redaelli G (2020) A meteorological–hydrological regional ensemble forecast for an early-warming system over small Apennine catchments in Central Italy. *Hydrol Earth Sys Sci* 24(6):3135–3156
- Friedl MA, McIver DK, Zhang XY, Hodges JCF, Schneider A, Bacinni A, Strahler AH, Cooper A, Gao F, Schaaf C, Liu W (2001) Global land cover classification results from MODIS. In: IGARSS 2001. Scanning the present and resolving the future. Proceedings. IEEE 2001 International Geoscience and Remote Sensing Symposium (Cat. No. 01CH37217) 2:733–735
- Gohil K, Jin MS (2019) Validation and improvement of the WRF building environment parametrization (BEP) Urban Scheme. *Climate* 7(9):109
- Hong SY, Lim JOJ (2006) The WRF single-moment 6-class microphysics scheme (WSM6). *Asia-Pac J Atmospheric Sci* 42(2):129–151
- Iannarelli AM, Di Bernardino A, Casadio S, Bassani C, Cacciani M, Campanelli M, Casasanta G, Cadau E, Diémoz H, Mevi G, Siani AM, Cardaci M, Dehn A, Goril P (2021) The Boundary-layer Air Quality-analysis Using Network of Instruments (BAQUNIN) supersite for Atmospheric Research and Satellite Validation over Rome area. *Bull Am Meteorol Soc* (published online ahead of print 2021)
- Janjić ZI (1994) The step-mountain eta coordinate model: further developments of the convection, viscous sublayer, and turbulence closure schemes. *Mon Weather Rev* 122(5):927–945
- Jin M, Dickinson RE, Zhang A (2005) The footprint of urban areas on global climate as characterized by MODIS. *J Clim* 18(10):1551–1565
- Keppas ChS, Papadogiannaki S, Parliari D, Kontos S, Poupkou A, Tzoumaka P, Kelessis A, Zanis P, Casasanta G, de' Donato F, Argentini S, Melas D (2021) Future climate change impact on urban heat island in two Mediterranean cities based on high-resolution regional climate simulations. *Atmosphere* 12:884
- Kumar R, Mishra V, Buzan J, Kumar R, Shindell D, Huber M (2017) Dominant control of agriculture and irrigation on urban heat island in India. *Sci Rep* 7(1):1–10
- Kusaka H, Chen F, Tewari M, Dudhia J, Gill DO, Duda MG, Wang W, Miya Y (2012) Numerical simulation of urban heat island effect by the WRF model with 4-km grid increment: an inter-comparison study between the urban canopy model and slab model. *J Meteor Soc Jpn Ser II* 90:33–45
- Lian J, Wu L, Bréon FM, Broquet G, Vautard R, Zaccaro TS, Dobler J, Pfister C (2018) Evaluation of the WRF-UCM mesoscale model and ECMWF global operational forecasts over the Paris region in the prospect of tracer atmospheric transport modeling. *Elementa: Sci Anthropocene* 6:64
- Litardo J, Palme M, Borbor-Cordova M, Caiza R, Macias J, Hidalgo-Leon R, Soriano G (2020) Urban Heat Island intensity and buildings' energy needs in Duran, Ecuador: Simulation studies and proposal of mitigation strategies. *Sustain Cities Soc* 62:102387
- Liu Y, Chen F, Warner T, Basara J (2006) Verification of a mesoscale data-assimilation and forecasting system for the Oklahoma City area during the Joint Urban 2003 field project. *J Appl Meteorol Climatol* 45(7):912–929
- Lo CP, Quattrochi DA (2003) Land use and land-cover change, urban heat island phenomenon, and health implications. *Photogramm Eng Remote Sens* 69(9):1053–1063
- Martilli A, Clappier A, Rotach MW (2002) An urban surface exchange parameterisation for mesoscale models. *Boundary Layer Meteorol* 104(2):261–304
- Mastrantonio G, Fiocco G (1982) Accuracy of wind velocity determinations with Doppler sodars. *J Appl Meteorol* 21(6):823–830
- Mastrantonio G, Argentini S, Viola A (1994) A New PC-based real time system to analyze sodar-echoes. *Italian Res Antarctic Atmosphere Italian Phys Soc Bologna* 45:227–235
- Mlawer EJ, Taubman SJ, Brown PD, Iacono MJ, Clough SA (1997) Radiative transfer for inhomogeneous atmospheres: RRTM, a validated correlated-k model for the longwave. *J Geophys Res Atmos* 102(D14):16663–16682
- Morini E, Touchaé AG, Rossi F, Cotana F, Akbari H (2018) Evaluation of albedo enhancement to mitigate impacts of urban heat island in Rome (Italy) using WRF meteorological model. *Urban Clim* 24:551–566

- Moeng C-H, Cotton WR, Bretherton C, Chlond A, Khairoutdinov M, Krueger S, Lewellen WS, MacVean MK, Pasquier JRM, Rand HA, Siebesma AP, Stevens B, Sykes RI (1996) Simulations of a stratocumulus-topped planetary boundary layer: intercomparison among different numerical codes. *Bull Am Meteor Soc* 77:261–278
- O'Malley C, Piroozfar P, Farr ER, Pomponi F (2015) Urban Heat Island (UHI) mitigating strategies: a case-based comparative analysis. *Sustain Cities Soc* 19:222–235
- Offerle B, Grimmond C, Oke T (2003) Parameterization of net all-wave radiation for urban areas. *J Appl Meteorol* 42:1157–1173
- Oke TR (1973) City size and the urban heat island. *Atmos Environ* 7(8):769–779
- Oke TR (1988) The urban energy balance. *Prog Phys Geogr* 12(4):471–508
- Pichelli E, Ferretti R, Cacciani M, Siani AM, Ciardini V, Di Iorio T (2014) The role of urban boundary layer investigated with high-resolution models and ground-based observations in Rome area: a step towards understanding parameterization potentialities. *Atmos Meas Tech* 7(1):315
- Pielke RA Sr, Adegoke J, Beltraán-Przekurat A, Hiemstra CA, Lin J, Nair US, Niyogi D, Nobis TE (2007) An overview of regional land use and land-cover impacts on rainfall. *Tellus b: Chem Phys Meteorol* 59(3):587–601
- Pineda N, Jorba O, Jorge J, Baldasano JM (2004) Using NOAA AVHRR and SPOT VGT data to estimate surface parameters: application to a mesoscale meteorological model. *Int J Remote Sens* 25(1):129–143
- Rotunno R, Chen Y, Wang W, Davis C, Dudhia J, Holland GJ (2009) Large-eddy simulation of an idealized tropical cyclone. *Bull Am Meteor Soc* 90:1783–1788
- Satya BA, Shashi M, Pratap D (2020) Effect of temporal-based land use–land cover change pattern on rainfall runoff. In: Ghosh J, da Silva I (eds) *Applications of geomatics in civil engineering*. Lecture Notes in Civil Engineering, vol 33. Springer, Singapore
- Salamanca F, Martilli A, Tewari M, Chen F (2011) A study of the urban boundary layer using different urban parameterizations and high-resolution urban canopy parameters with WRF. *J Appl Meteorol Climatol* 50(5):1107–1128
- Salamanca F, Zhang Y, Barlage M, Chen F, Mahalov A, Miao S (2018) Evaluation of the WRF-urban modeling system coupled to Noah and Noah-MP Land surface models over a semiarid urban environment. *J Geophys Res Atmos* 123:2387–2408
- Siebesma AP, Brown CSBA, Chlond A, Cuxart J, Duynkerke P, Jiang H, Khairoutdinov M, Lewellen D, Moeng CH, Sanchez E, Stevens B, Stevens DE (2003) A large-eddy simulation study of shallow cumulus convection. *J Atmos Sci* 60:1201–1219
- Sharma A, Fernando HJ, Hellmann J, Chen F (2014) Sensitivity of WRF model to urban parameterizations, with applications to Chicago metropolitan urban heat island. In: *Fluids Engineering Division Summer Meeting*, 46247, V01DT28A002, American Society of Mechanical Engineers
- Skamarock W, Klemp JB, Dudhia J, Gill DO, Liu Z, Berner J, Wang W, Powers JG, Duda MG, Barker DM, Huang XY (2019) A description of the advanced research WRF model version 4, National Center for Atmospheric Research: Boulder, CO, USA
- Solecki WD, Rosenzweig C, Parshall L, Pope G, Clark M, Cox J, Wiencke M (2005) Mitigation of the heat island effect in urban New Jersey. *Glob Environ Change Part b: Environ Hazards* 6(1):39–49
- Sozzi R, Casasanta G, Ciardini V, Finardi S, Petenko I, Cecilia A, Argentini S (2020) Surface and aerodynamic parameters estimation for urban and rural areas. *Atmosphere* 11:147
- Stewart ID, Oke TR (2012) Local climate zones for urban temperature studies. *Bull Am Meteorol Soc* 93(12):1879–1900
- Stoll R, Portè-Agel F (2009) Surface heterogeneity effects on regional scale fluxes in stable boundary layers: Surface temperature transitions. *J Atmos Sci* 66:412–431
- Sugawara H, Takamura T (2014) Surface albedo in cities: case study in Sapporo and Tokyo, Japan. *Boundary-Layer Meteorol* 153(3):539–553
- Sun Y, Wang S, Wang Y (2020) Estimating local-scale urban heat island intensity using night-time light satellite imageries. *Sustain Cities Soc* 102125
- Tan J, Zheng Y, Tang X, Guo C, Li L, Song G, Chen H (2010) The urban heat island and its impact on heat waves and human health in Shanghai. *Int J Biometeorol* 54(1):75–84
- UN (2018) Department of Economic and Social Affairs, Population Division: *World Urbanization Prospects (WUP): The 2018 Revision, Methodology*
- Wang Y, Berardi U, Akbari H (2016) Comparing the effects of urban heat island mitigation strategies for Toronto, Canada. *Energy Build* 114:2–19
- Witiw MR, Baars J, Fischer K (2003) Urban influences on visibility. In: *Proceedings of the 5th international conference on urban climate*, pp 1–5
- Wu S, Mickley LJ, Kaplan JO, Jacob DJ (2012) Impacts of changes in land use and land cover on atmospheric chemistry and air quality over the 21st century. *Atmos Chem Phys* 12(3):1597–1609

Zhang H, Jin MS, Leach M (2017) A study of the Oklahoma city urban heat island effect using a WRF/single-layer urban canopy model, a Joint Urban 2003 field campaign, and MODIS satellite observations. *Climate* 5:72

**Publisher's Note** Springer Nature remains neutral with regard to jurisdictional claims in published maps and institutional affiliations.